UNIVERSITY OF CALIFORNIA

DEPARTMENT OF MECHANICAL ENGINEERING

DAVIS, CALIFORNIA

FINAL REPORT

for

Joint Research Interchange

entitled

AN INVESTIGATION OF TURBULENCE
STRUCTURE IN A LOW REYNOLDS NUMBER
INCOMPRESSIBLE TURBULENT BOUNDARY

B.R. White, Principal Investigator
C.J. Strataridakis, Graduate Research Assistant

NASA Grant Number NCA2-79

prepared for

Experimental Fluid Dynamics Branch
NASA Ames Research Center
Moffett Field, California 94035

May 1987

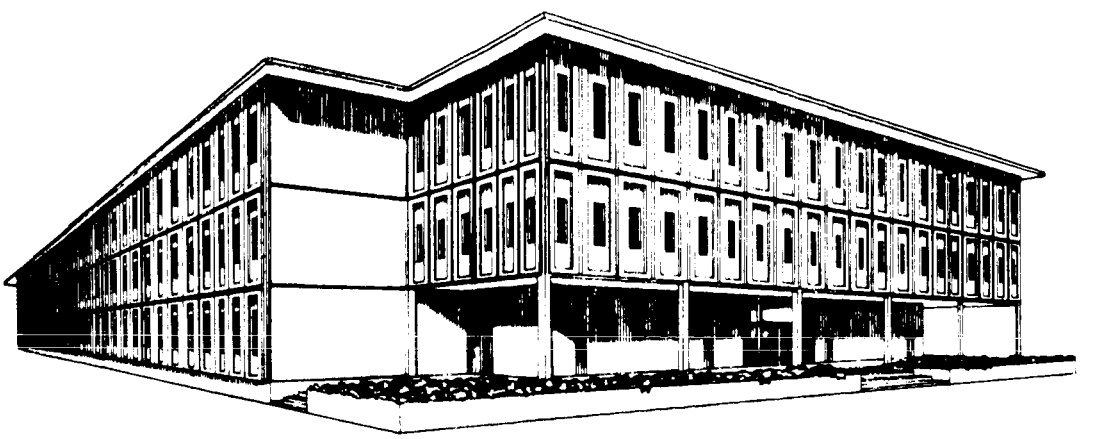

FINAL REPORT

for

Joint Research Interchange

entitled

AN INVESTIGATION OF TURBULENCE STRUCTURE IN A LOW-REYNOLDS-NUMBER INCOMPRESSIBLE TURBULENT BOUNDARY

B.R. White, Principal Investigator
C.J. Strataridakis, Graduate Research Assistant

NASA Grant Number NCA2-79

prepared for

Experimental Fluid Dynamics Branch
NASA Ames Research Center
Moffett Field, California 94035

May 1987

ABSTRACT

An existing high turbulence intensity level (5%) atmospheric boundary-layer wind-tunnel has been succesfully converted to a relatively low level turbulence (0.3%) wind tunnel through extensive modification, testing and calibration. A splitter plate was designed, built, and installed into the wind-tunnel facility to create thick, mature, two-dimensional turbulent boundary layer flow at zero pressure gradient. Single and cross hot-wire measurements show turbulent boundary layer characteristics of good quality with unsusually large physical size, i.e., viscous sublayer of the order of 1 mm high. These confirm the potential ability of the tunnel to be utilized for future high-quality near-wall turbulent boundary layer measurements. It compares very favourably with many low turbulence research tunnels.

Figure Captions

Figure 5. Mean velocity and percent turbulence-level profiles at the middle of the test section without the splitter plate.

Figure 6. Modified for low-turbulence-level UCD Atmospheric Boundary Layer Wind Tunnel with the splitter plate in place.

Figure 7. Full scale leading edge of the splitter plate.

Figure 8. Splitter plate support assembly.

Figure 9. Splitter plate in the wind tunnel (front view).

Figure 10. Mean velocity and root-mean-square velocity profiles downstream the entrance section of the wind tunnel (centerline).

Figure 11. Mean velocity and root-mean-square velocity profiles downstream the entrance section of the wind tunnel (1 ft off-centerline).

Figure 12. Mean velocity profile 2 ft downstream the trailing edge of the splitter plate.

Figure 13. Root-mean-square velocity profile 2 ft downstream the trailing edge of the splitter plate.

Figure 14. Mean and root-mean-square velocity profiles 2 ft downstream the trailing edge of the splitter plate.

Figure 15. Longitudinal pressure gradient determination in the vicinity of the near-wall measurement site.

Figure 16. Splitter plate undulation determination using a single hot-wire (longitudinal).

Figure 17. Splitter plate undulation determination using a single hot-wire (tranverce).

Figure 18. Single hot-wire placed over the splitter plate for near-wall measured.

Figure 19. Near-wall positioning mechanism.

Figure 20. TSI calibrator (model # 1125) with a straight single hot-wire probe mounted.

Figure 21. Single hot-wire calibration using LDV.

Figure 22. LDV calibration curves for the TSI calibrator. Line is

Table 1. Turbulent boundary layer characteristics.

Contents

I. Introduction

The present work was conducted at UC Davis and the primary goal was to convert the existing Atmospheric Boundary-Layer Wind Tunnel to a low turbulence level tunnel for the purposes of high quality near-wall turbulence measurements. This wind-tunnel facility is very important because of its capability of producing thick turbulent boundary layers, which increases the measurement resolution. Low speed is a characteristic of the UCD tunnel, therefore, the turbulent structures have large time scales, which provide the opportunity for easier, more detailed turbulence measurements and observations.

In preparation for the detailed turbulence studies, a prototype splitter plate was designed, built, and installed in the wind tunnel. Finally, the turbulent boundary layer created by the splitter plate was characterized by experiment.

Measurements were made using a Pitot-static tube, a single hot-wire probe, and a cross-wire probe of the boundary-layer type. An accurate probe positioning mechanism was designed and built for high quality near-wall measurements.

A Cyborg ISAAC-2000 state-of-the-art data acquisition system was used. Data reduction computer systems were programmed in Lattice "C" for fast acquisition and efficient on-line data analysis.

Finally, the present experimental results were compared with classical results.

II. Experimental Facilities and Procedures

Wind Tunnel

In the present study the UCD Atmosheric Wind-Tunnel Facility was used. The tunnel was an open-return type and its overall length was 70 ft. The entrance section had a bell mouth shape with a contraction area of 4:1 (Figure 1). The flow development section was 40 ft long and had divergent walls to reduce the streamwise pressure gradient. The test section was 8 ft long, 5.5 ft high, and 4 ft wide. The ceilings of the flow development and test sections were adjustable for longitudinal pressure gradient control. The present test configuration provided zero-pressure-gradient flow. Access to the test section was through a framed Plexiglas door 3/4" thick (7.5 ft X 3.5 ft). Six clamps on each top and bottom of the door, as well as two large clamps at

each end were used to seal the door. Additional sealing was achieved by the use of heavy-duty adhesive foam tape, which was glued on the test section door-rim and provided an air-tight seal when the door was closed for testing.

In the test section a three-dimensional probe positioning mechanism (Figures 2 and 3) provided fast and accurate (within .05") sensor placement. The scissor arms of the mechanism, which provided vertical probe motion, were made of aerodynamically shaped struts to minimize flow disturbances.

The diffuser section was 8 ft long and had an expansion area that provided a continuous transition from the rectangular cross-sectional area of the test section to the circular cross-sectional area of the fan. To eliminate upstream fan swirl effects and avoid flow separation in the diffuser section, a large scale fiberboard honeycomb and smaller aluminum Wexcel honeycomb (3/4" X 6") were placed between the fan and diffuser sections.

The fan had eight constant pitch, 6 ft diameter blades (Figure 4). The variable speed 10 hp DC-motor drove the blades with a belt and pulley system.

Originally, the atmospheric wind tunnel was designed to generate artificially thickened rough-wall boundary layers. The free-stream turbulence was approximately 5.0 %.

In preparation for the detailed turbulence studies, the boundary layer in the UCD Atmospheric Wind Tunnel had to be tuned to insure two-dimensional flow and low free-stream turbulence levels. The entrance of the wind tunnel was modified for flow conditioning as follows: First, two 1/20" mesh stainless steel screens were placed at the bell mouth of the entrance (81" X 119"). Second, a 3/8" X 6" aluminum Hexcel honeycomb was mounted at the begining of the long flow development section, followed by four 1/20" mesh stainless-steel screens. The mean flow characteristics (streamwise velocity and turbulence profiles along the tunnel centerline) were measured in the middle of the test section using a single hot-wire sensor (Figure 5). Additional screens (up to eight) located at the beginning of the flow development section were tested and no significant changes in the mean flow characteristics were observed. As Figure 5 indicates the free-stream turbulence level at this point was reduced to about 2.5 % with no high pass electronic filtering.

Performing spectral analysis to the instantaneous raw hot-wire voltages there was observed a very low frequency voltage signal about 8 Hz. This was evidently caused by a mass of air circulating between the open-return wind tunnel and the room. A series of (11" X 11" by 2 ft long) open cardboard boxes were stacked outside the entrance of the wind tunnel, and thousands of small (6" high) wooden wedges suspended on the two wall surfaces neighbouring the exit of the tunnel (Figure 6) reduced the free-

stream turbulence to 0.3 %.

Splitter Plate

The 3/16" thick by 24 ft long aluminum splitter plate which spanned the width of the wind tunnel was installed in the wind tunnel. The splitter plate had an axe-shaped leading edge (Figure 7). The cross-section of the leading edge formed an isosceles triangle, which had an 1/16" rounded leading-edge convex and a 3" height.

The splitter plate consisted of two separate aluminum plates. Both plates were rested horizontally on seven equally spaced 1.5" X 1.5" aluminum right-angle ribs (Figure 8). Each side of these ribs was bolted on a 22 ft aluminum channel. The channels were bolted on the two vertical wind-tunnel walls. The surface of the splitter plate was alligned horizontally with the tunnel floor at a height of 2 ft (Figure 9).

After the splitter plate was carefully mounted in the tunnel, the new flow conditions downstream the entrance section and in the test section were measured: At 21" downstream of the last screen two velocity and turbulence profiles were surveyed, one at the tunnel centerline and the other at 1 ft off-center

(Figures 10 and 11). One foot upstream the trailing edge of the plate, near-wall measurements were made (refer to **Presentation of Results**). Finally, at two feet downstream the trailing edge,the wake of the plate measurements were performed (Figures 12 to 14).

The longitudinal pressure gradient in the region of the near-wall measurement site was determined (Ue*dUe/dx) by moving a single hot-wire probe along the test-section centerline at free-stream heights and measure the velocities. The probe was mounted on the three dimensional traversing mechanism. Similarly, the traverse pressure was examined. Both pressure gradients were experimentally found to be zero (Figure 15).

The undulating surface of the plate was examined by traversing the probe in the longitudinal and tranverse directions near the wall. The testing height was 0.25 inches. Figures 16 and 17 present the results. The calculated maximum plate deformation at the center was 0.0005 inches.

Near-Wall Probe Positioning Mechanism

For reliable near-wall measurements, it was important to know accurately the height of the hot-wire sensor. A "Starrett, No. 63" micrometer (resolution of 0.0001") was used.

The hot-wire probe (a TSI straight probe, model # 1210) was connected to a TSI 36 inch vertical support through an 80 degree angle probe adapter as shown in Figure 18. Thus, the centerline of the single probe made a 10 degree angle with the wall.

The vertical support was passing through the plate and wind-tunnel floor, and securely attached to the probe positioning mechanism using nut locks (Figure 19). Finally, the vertical movement of the probe was performed by changing the micrometer dial to the next prescribed position.

Hot-Wire Sensor Calibrator

For the single and cross hot wires the TSI calibrator, model 1125, was used. In the present study, since the near wall velocities were within the range of 0.3 to 3.0 m/s (refer to section 5) the low velocity nozzle of the TSI calibrator was used (Figure 20).

The nozzle calibration data were supplied by TSI. However, a LDV precalibrated hot-wire sensor (Figure 21, for this calibration the LDV system of the UCD combustion lab was incorporated), was used to verify the TSI nozzle calibration. Figure 22 shows excellent aggreement between the LDV measurements

and TSI data.

The nozzle made by Strataridakis [ref. 4] was calibrated by using a LDV precalibrated boundary-layer type hot-wire probe. Figure 22 includes the calibration. This nozzle was used for low velocity X-probe calibration (Figures 23 and 24).

III. Instrumentation

The constant temperature hot-wire anemometer analog signals were conditioned with the eighth-order elecronic low-pass filters (DYNAMICS). The cutoff frequency of the filters was 80 Hz, which well satisfied the sampling theorem.

The fluctuating raw anemometer voltages were observed through a Teckronix four-channel oscilloscope during the testing period. A Nicolet-660A digital spectrum analyzer was used to inspect the voltage power spectrum during data acquisition.

The data was acquired by the Cyborg ISAAC-2000 12-bit, four

channel simultaneous data acquisition system (expandable to 32 channels). The maximum achievable sampling rate was 200 KHz. In this experiment all the measurements were made at sampling frequency of 500 Hz. For every data point the long-time statistics were performed as the average of 25,000 individual samples.

The data acquisition triggering and the in-parallel sample transfer from ISAAC-2000 to the 640 Kbyte RAM of the IBM-PC/AT computer was performed using the programming language "Lattice-C". All the data analysis was on-line executed using the RAM of the computer. An instrumentation block diagram is shown in Figure 25.

IV. Presentation of Results

In this section the near-wall measurements will be presented. All the experimental points plotted were the original long-time averaged (25,000 samples at 500 Hz sampling rate) raw data, except the data very close to the wall ($y^+ < 5$) which has been corrected to account for the heat transfer effects from the hot-wire to the thermally conducting aluminum surface of the plate (Wills 1962, Bhatia et. al. 1982).

A typical mean velocity profile at a Reynolds number of 2.5 million based upon distance from the leading edge of the plate is shown in Figure 26. The velocities and heights had been nondimensionalized by the freestream velocity and boundary layer thickness respectively. The freestream velocity was measured continuously with a pitot-static tube positioned at the center of the test section, at the same downstream location with the hot-wire near the wall.

The near wall detail of another velocity distribution is shown in Figure 27 along with the line tangent to the viscous sublayer profile. The slope of this line yields a skin friction coefficient estimation of 0.00326. The following Figure 28 presents the viscous sublayer of the previous profile. The equation of this line was found by a linear regration analysis through 14 experimental data points and using the non-slip wall boundary condition.

Figure 29 includes a plot of the turbulence profile as it compared with the classical data by Klebanoff 1955. This profile was measured by a single hot wire. The near wall detail of the turbulence distribution is presented in Figure 30. There is reasonable aggreement with Klebanoff's results.

The X-probe turbulence level data is plotted in Figure 31 along with Klebanoff's measurements. The present results

showed lower values in the y-component of turbulence distribution.

Figure 32 shows the Clauser method for determining Cf applied to the present data. The estimated Cf had a value of 0.0031 which is close to the value determined from the slope of the viscous sublayer profile.

The u+ versus log10[y+] mean velocity profile is graphed in Figure 33. The universally accepted "law of the wall" line is included along with the linear viscous sublayer u+ = y+ curve. The aggreement with these "laws" is good. The window plot presents data of Reichardt (channel) and Laufer (pipe) [ref. 5].

Two velocity profiles measured at different times are plotted in Figure 34. The small discrepancy in the near-wall region was due to the initial height positioning of the hot-wire sensor (for the first profile magnifying lens along with feeler gauges were used, while for the second profile only magnifying lens was used).

In Figure 35 the urms+ versus log10[y+] data is shown along with the flat plate measurements of Haritonidis [ref. 2]. The aggreement is reasonable.

The local turbulence intensities are presented in Figure 36 with the channel flow measurements of Eckelmann and the solutions

of the full Navier-Stokes solved by Kim et. al. [ref. 3]. The present data shows similarity with Echelmann's data however, the former have higher values than the latter. Using the present data l' Hospital's rule was applied at the wall and a value of 37% local turbulence levelwas calculated. This value is in good aggreement with the numerical solutions of data of Kim et. al. 1987. Figure 37 shows a magnified detail of the present local turbulence measurements. Haritonidis, (personal communication) found an independent of y+ value of 40% local turbulence intensity in the near wall region.

Figure 38 includes the present X-probe shear-stress data as they compared with Klebanoff's shear-stress data. The aggreement is good. Figure 39 is the cross correlation coefficient data compared with Klebanoff's results.

The scewness and flatness profiles in the near wall region is shown in Figure 40 with the experimental data of Echelmann, and the numerical simulation data of Kim et.al. 1987.

Typical values of the flat plate boundary layer produced in the modified UCD Atmospheric Boundary Layer Wind Tunnel are summarized in Table 1.

V. Conclusions/Summary

The UCD Atmospheric Boundary Layer Wind Tunnel was used for the turbulence investigation in the near wall region. Originaly, the wind tunnel was designed to create thick turbulent boundary layers with usual high-freestream turbulence level (approximately 5%).

The first task of the present study was to "clean-up" the flow, i.e., to convert the tunnel to a low turbulence one. New aluminum honeycombs replaced the old PVC-tubing flow straighteners at the entrance of the long flow development section and at the end of the test section. Six turbulence reducing screens were added after the entrance section. More screens were tested, however, there was no further inprovement in the flow. These changes reduced the level of turbulence to 2.5%. The turbulence level was decreased to 0.3% by covering the room walls adjacent to the exit of the wind tunnel with wooden spikes and by further conditioning the flow at the entrance and exit.

The second goal of the present study was to design and install a long splitter plate within the tunnel, in order to

create thick, mature, two-dimensional turbulent boundary layer. The spitter plate consisted of two 3/16" thick aluminum 12 ft plates thus having a total length of 24 ft. Sevel horizontal aluminum ribs supported the plate allowing for minimal plate deflection (less than 0.0005"). The pressure gradient was adjusted to zero by properly inclining the tunnel's false ceiling.

The third objective of the present study was to take mean turbulence measurements and, therefore, find the parameters that characterize the flow. Table 1 presents these characteristics. The turbulence data agree reasonably well with classical data [ref. 1]. Near-wall measurements show strong agreement with newly published numerical solutions and recent experimental data [ref. 2 and 3].

In conclusion, the low-turbulence-level Atmospheric Boundary Layer Wind Tunnel facility at UCD, in connection with the state of the art instrumentation available have demonstrated through the present experimental data that the UCD tunnel is suitable for studying near-wall turbulence structure in an incompressible turbulent boundary layer.

References

[1] Klebanoff, P.S., 1955 "NACA Report 1247".

[2] Johanson, Her, Haritonidis, JFM 1987, "On the Generation of High Amplitute Wall Pressure Peaks in Turbulent B.L. and Spots".

[3] Kim J., Moin P., Moser R., JFM 1987, "Turbulence Statistics in Fully Developed Channel Flow at Low Reynolds Number".

[4] Strataridakis C.J., UCD MS Thesis 1984, "Hot-Wire Anemometry Measurement of Turbulent Boundary Layer Flow Past a Two Dimensional Obstacle".

[5] Hinze, McGraw Hill 2nd Edition 1975, "Turbulence".

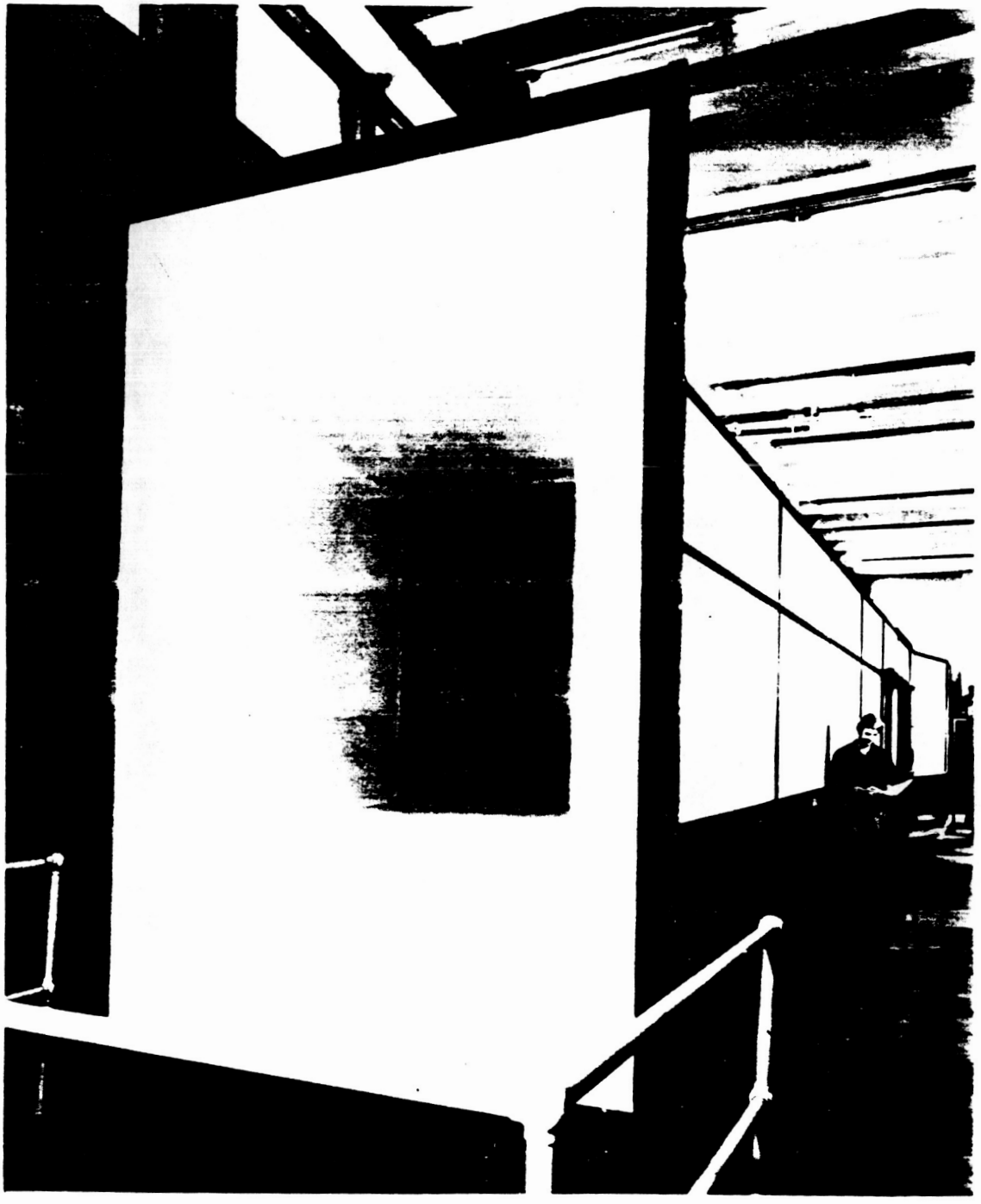

Figure 1 View of the Atmospheric Boundary Layer Wind Tunnel Facility before the turbulence-reduction modifications were installed.

Figure 2 View of the test section of the wind tunnel before installation of the splitter plate.

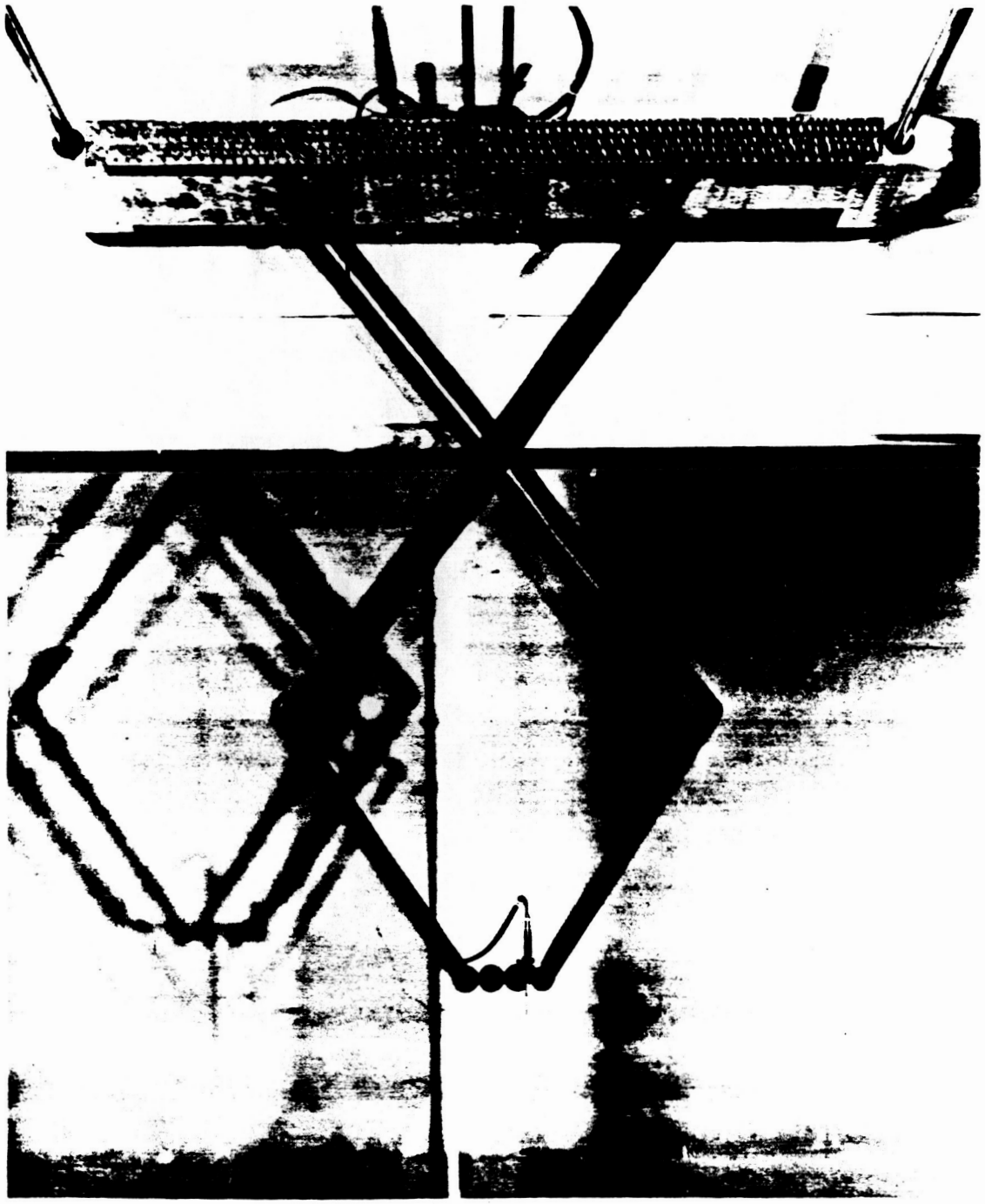

Figure 3 View of the three-axes probe system located in the test section of the wind tunnel.

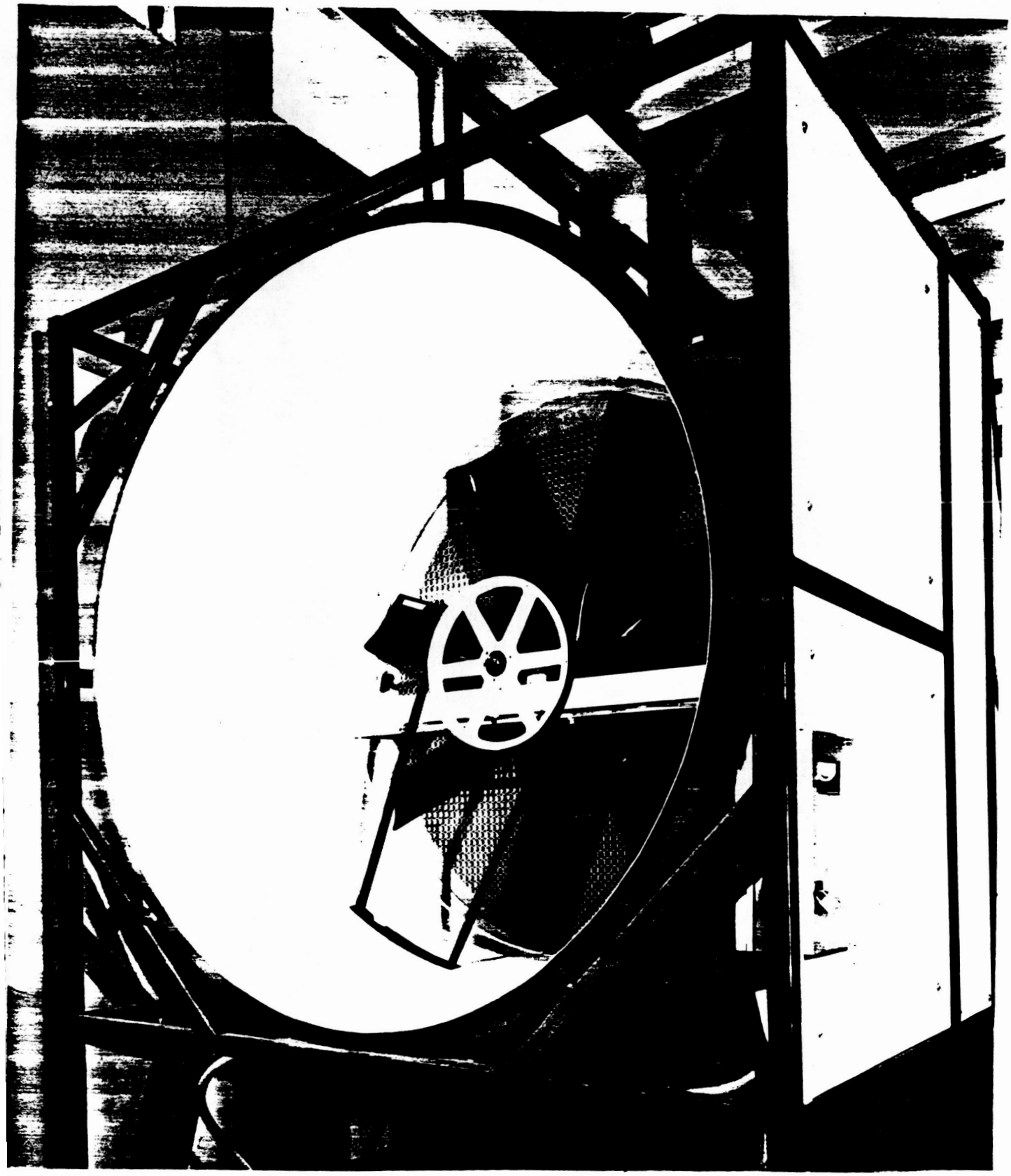

Figure 4 View of the diffuser-exit sections displaying the six-foot diameter fan blades.

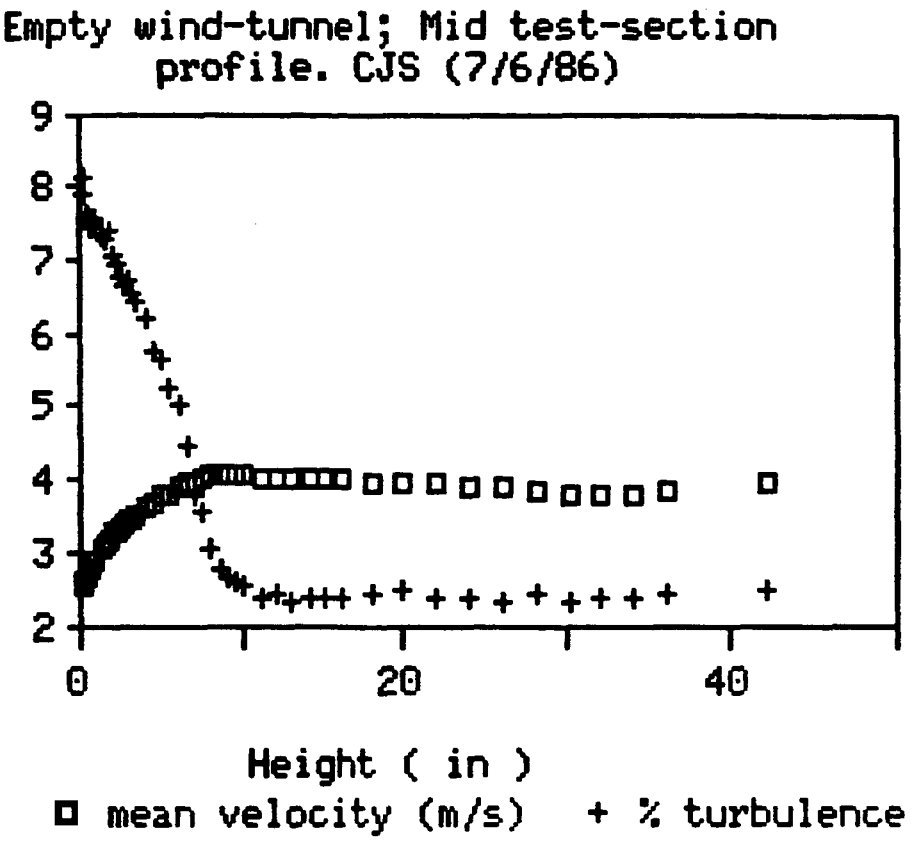

Figure 5. Mean velocity and percent turbulence-level profiles at the middle of the test section without the splitter plate.

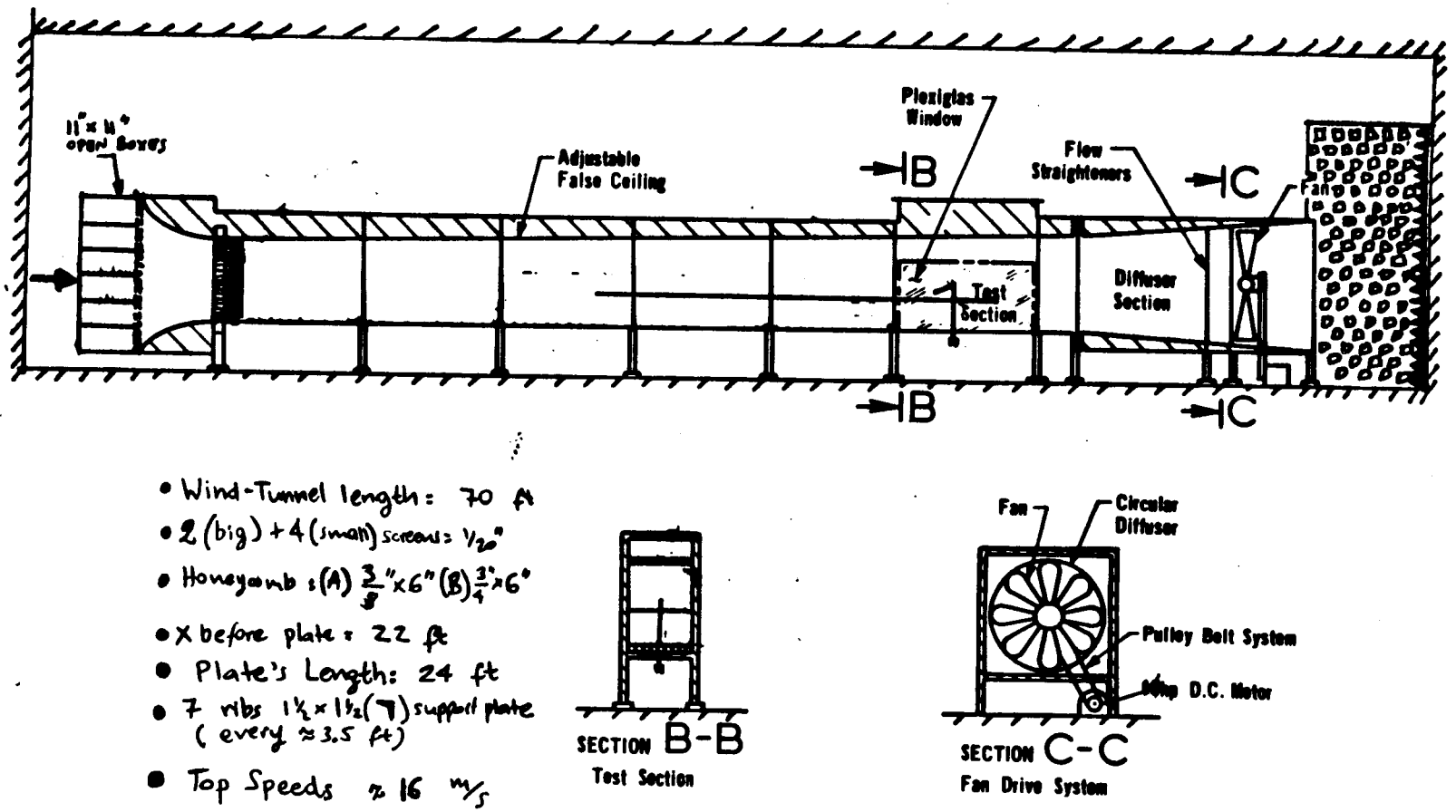

Figure 6. Modified for low-turbulence-level UCD Atmospheric Boundary Layer Wind Tunnel with the splitter plate in place.

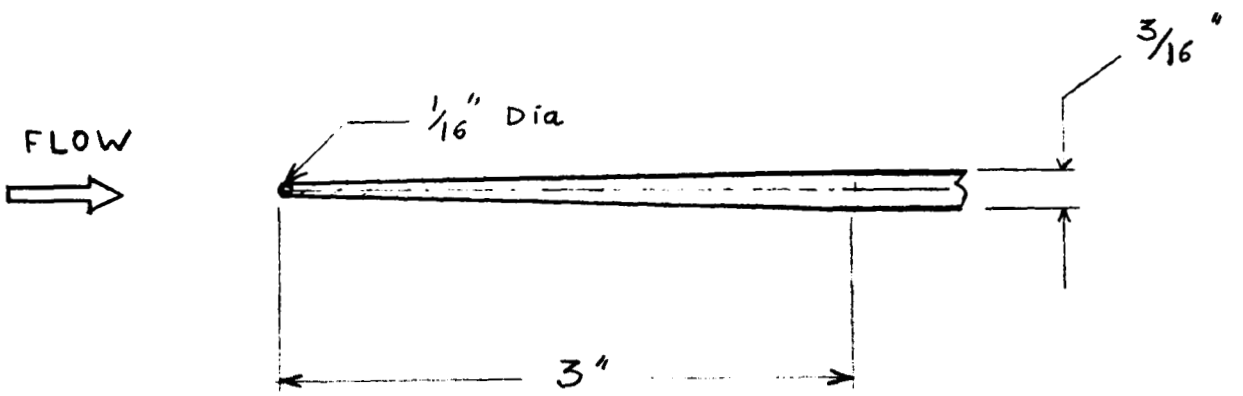

Figure 7. Full scale leading edge of the splitter plate.

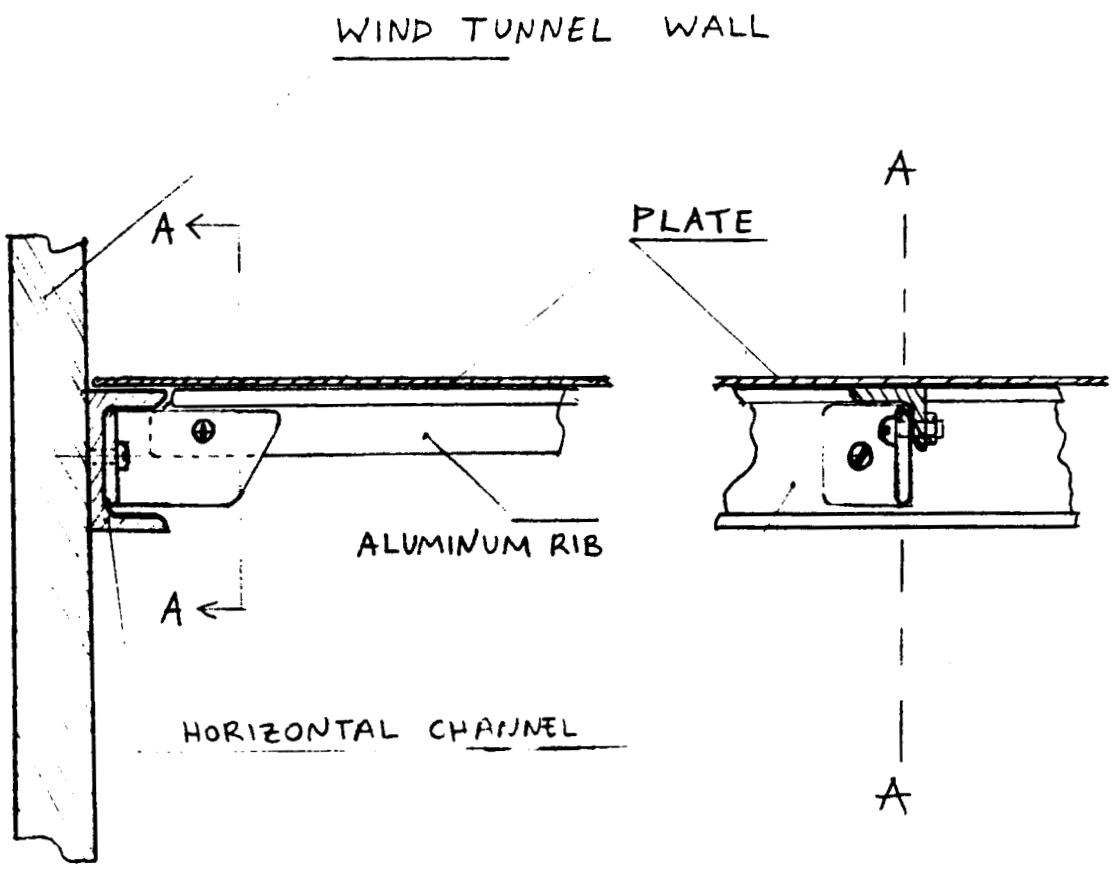

Figure 8. Splitter plate support assembly.

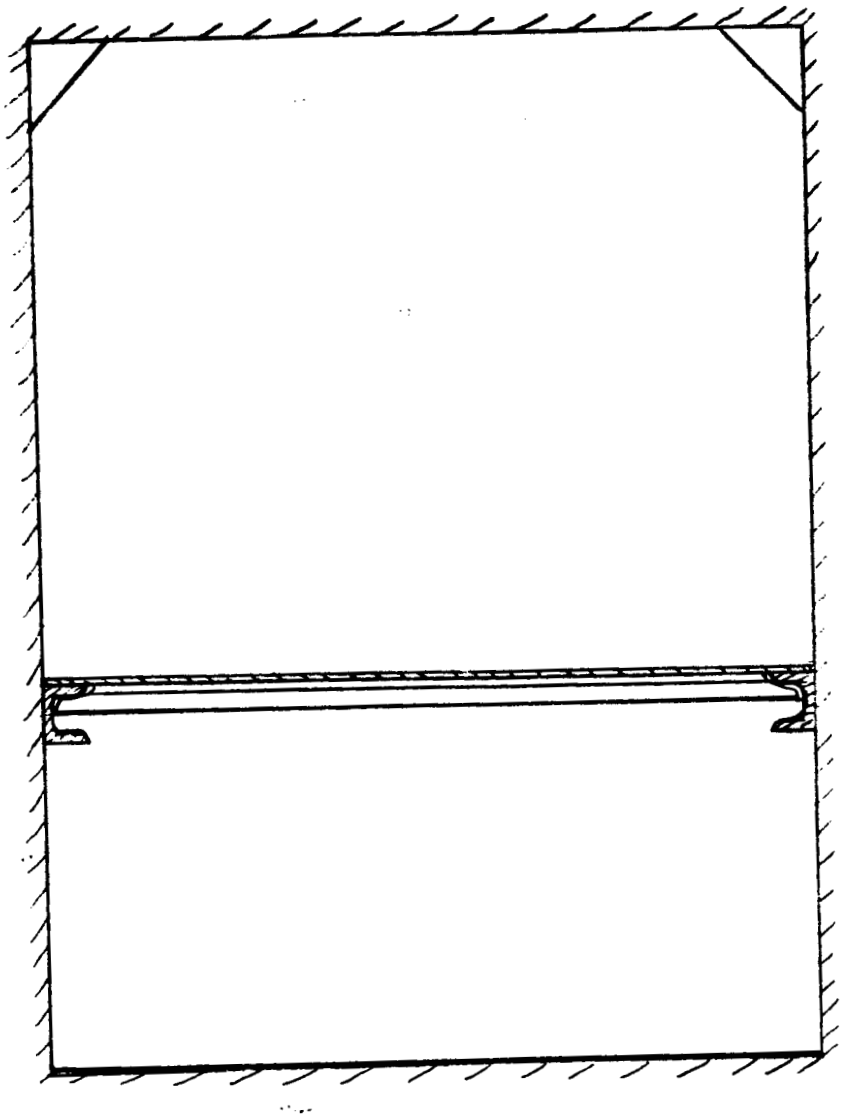

Figure 9. Splitter plate in the wind tunnel (front view).

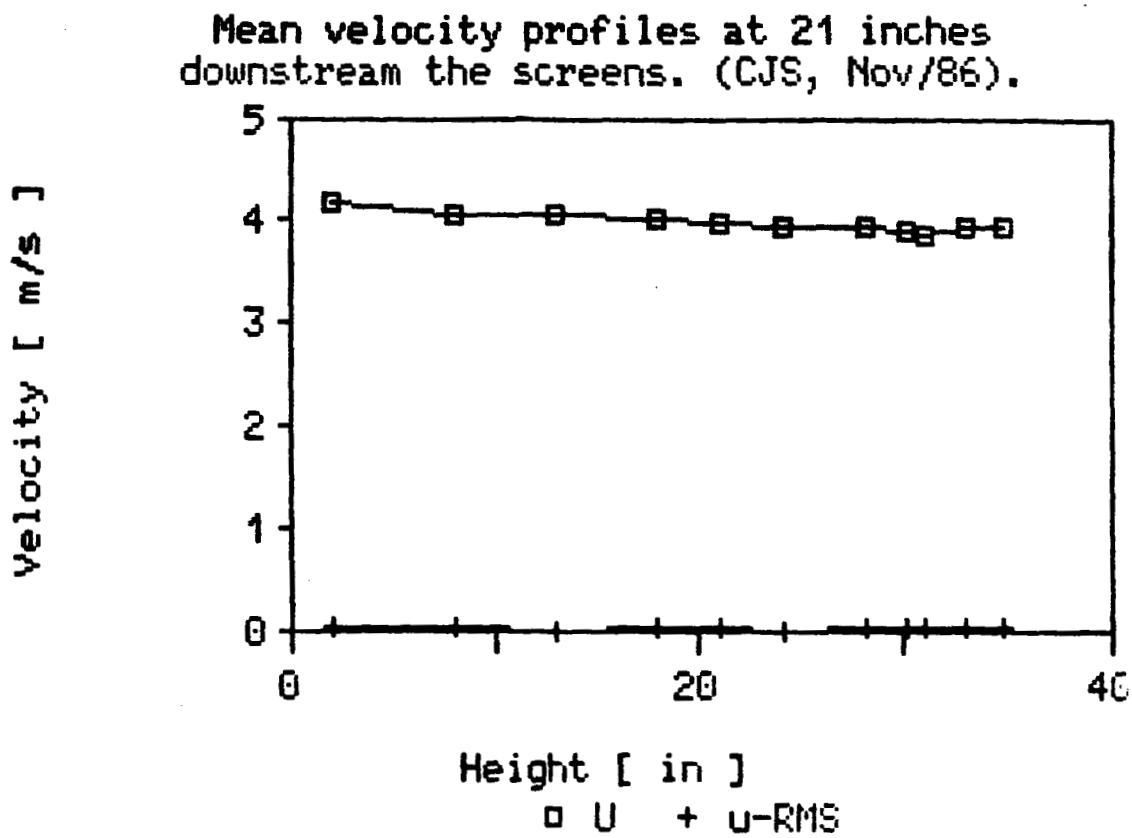

Figure 10. Mean velocity and root-mean-square velocity profiles downstream the entrance section of the wind tunnel (centerline).

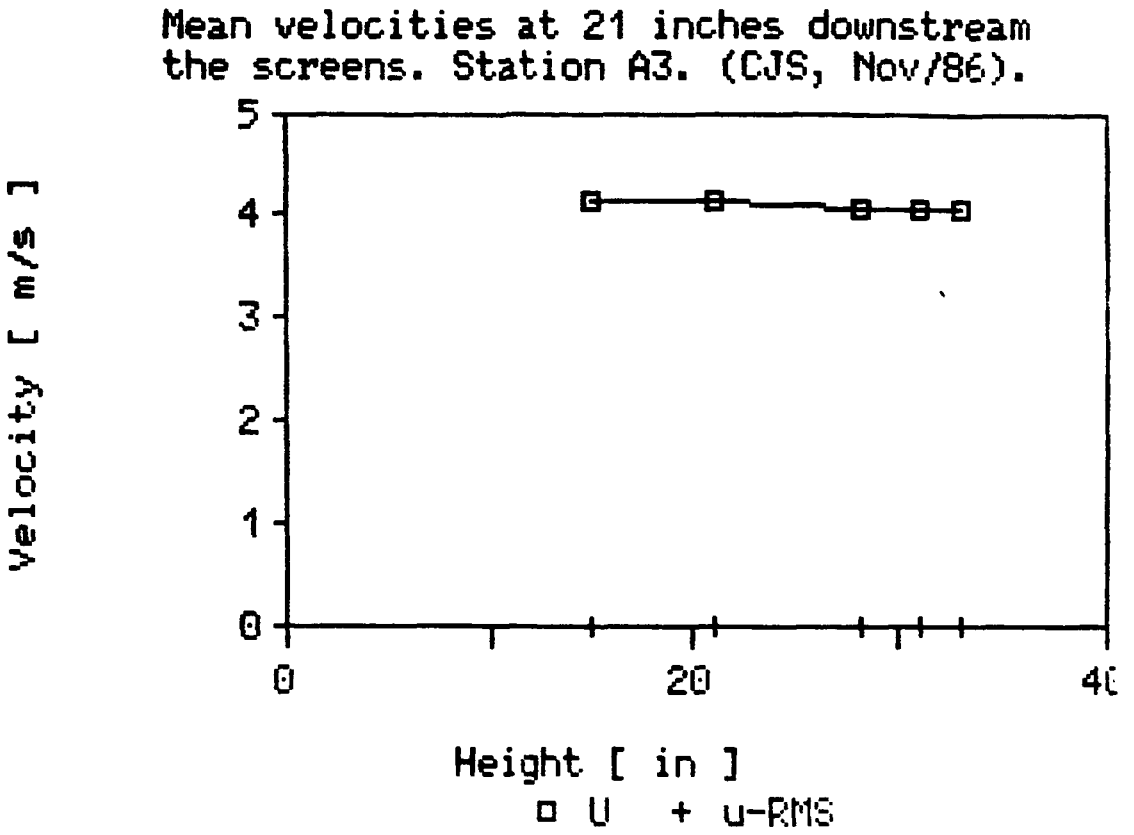

Figure 11. Mean velocity and root-mean-square velocity profiles downstream the entrance section of the wind tunnel (1 ft off-centerline).

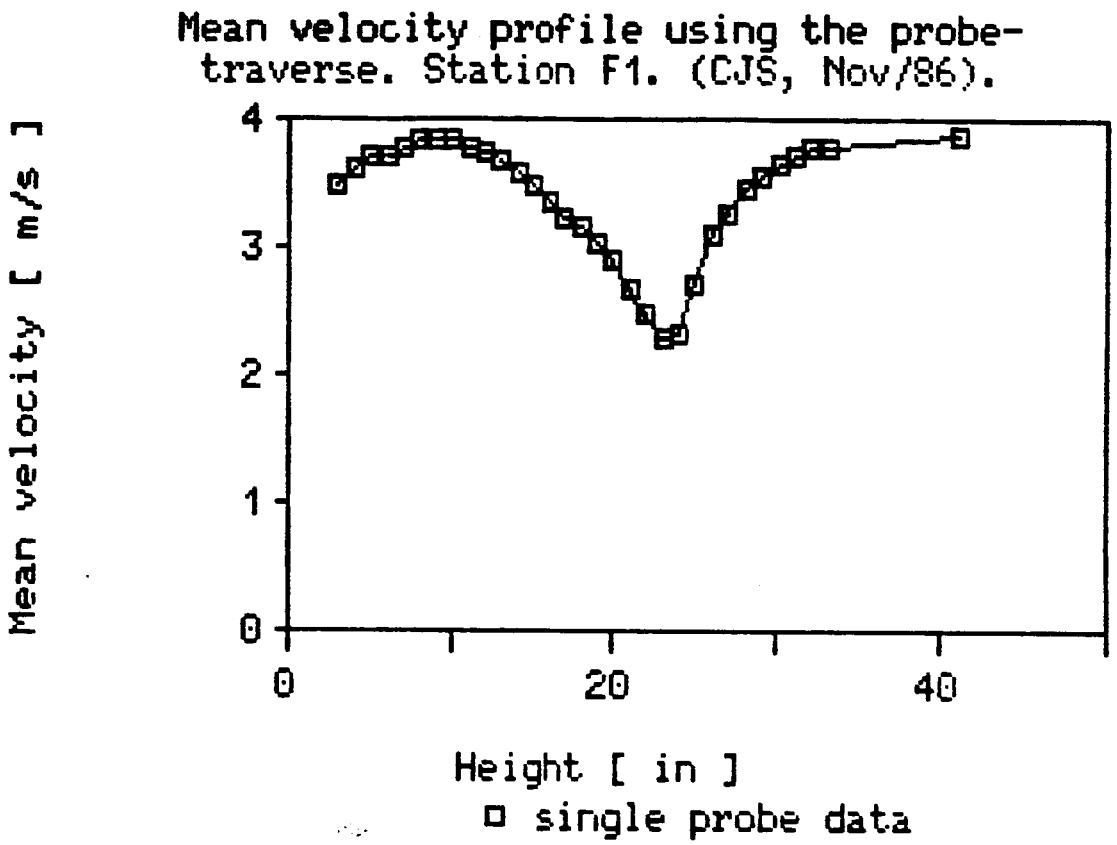

Figure 12. Mean velocity profile 2 ft downstream the trailing edge of the splitter plate.

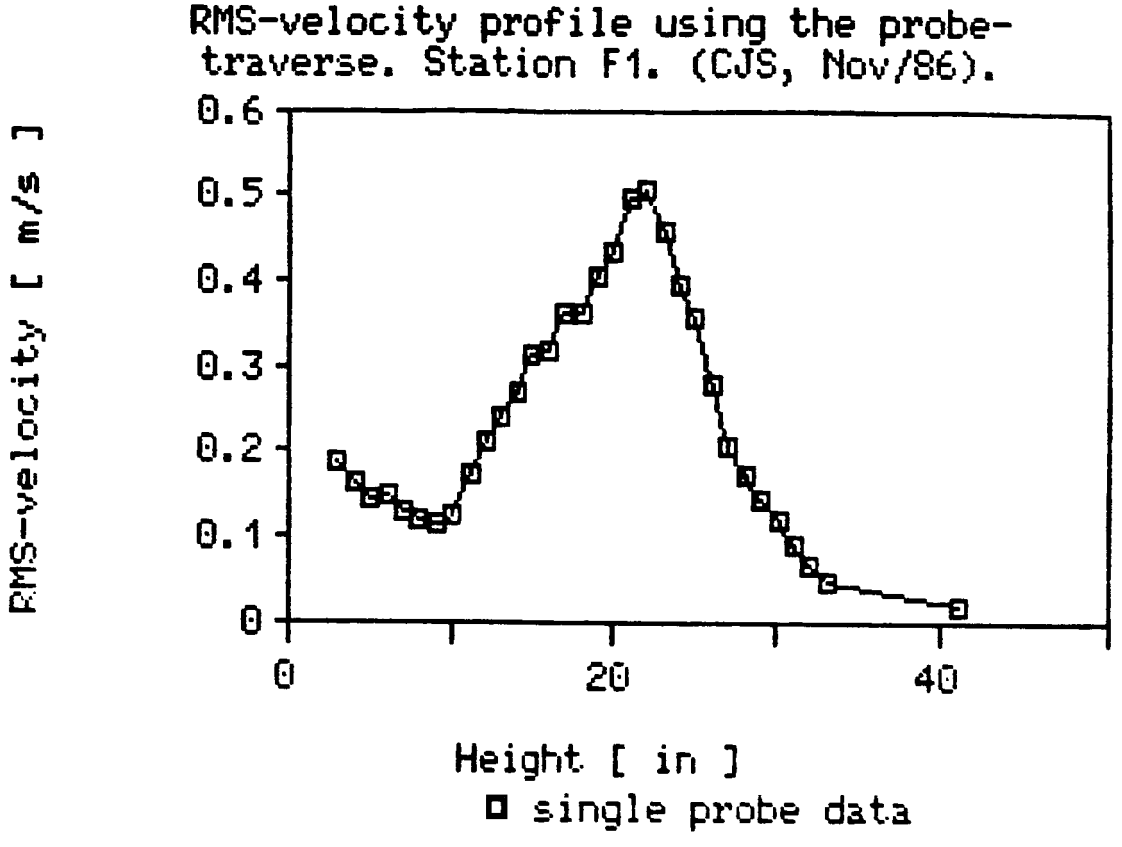

Figure 13. Root-mean-square velocity profile 2 ft downstream the trailing edge of the splitter plate.

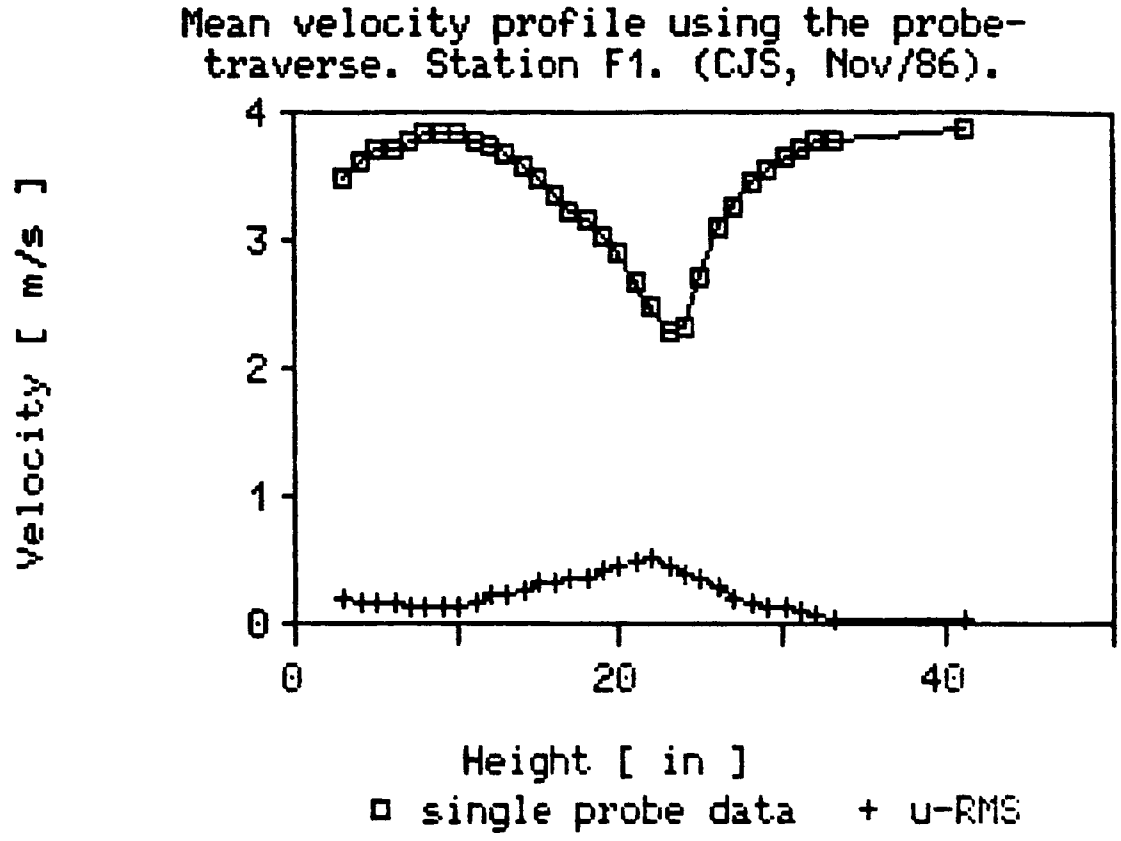

Figure 14. Mean and root-mean-square velocity profiles 2 ft downstream the trailing edge of the splitter plate.

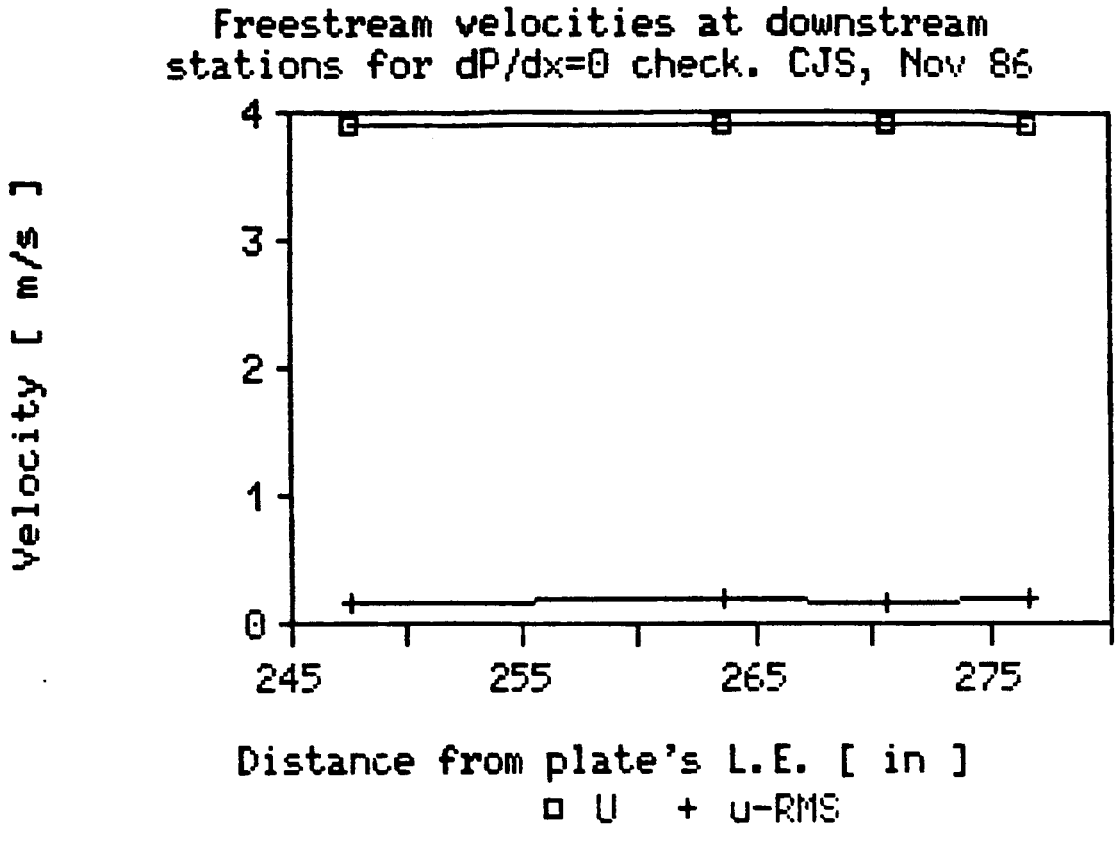

Figure 15. Longitudinal pressure gradient determination in the vicinity of the near-wall measurement site.

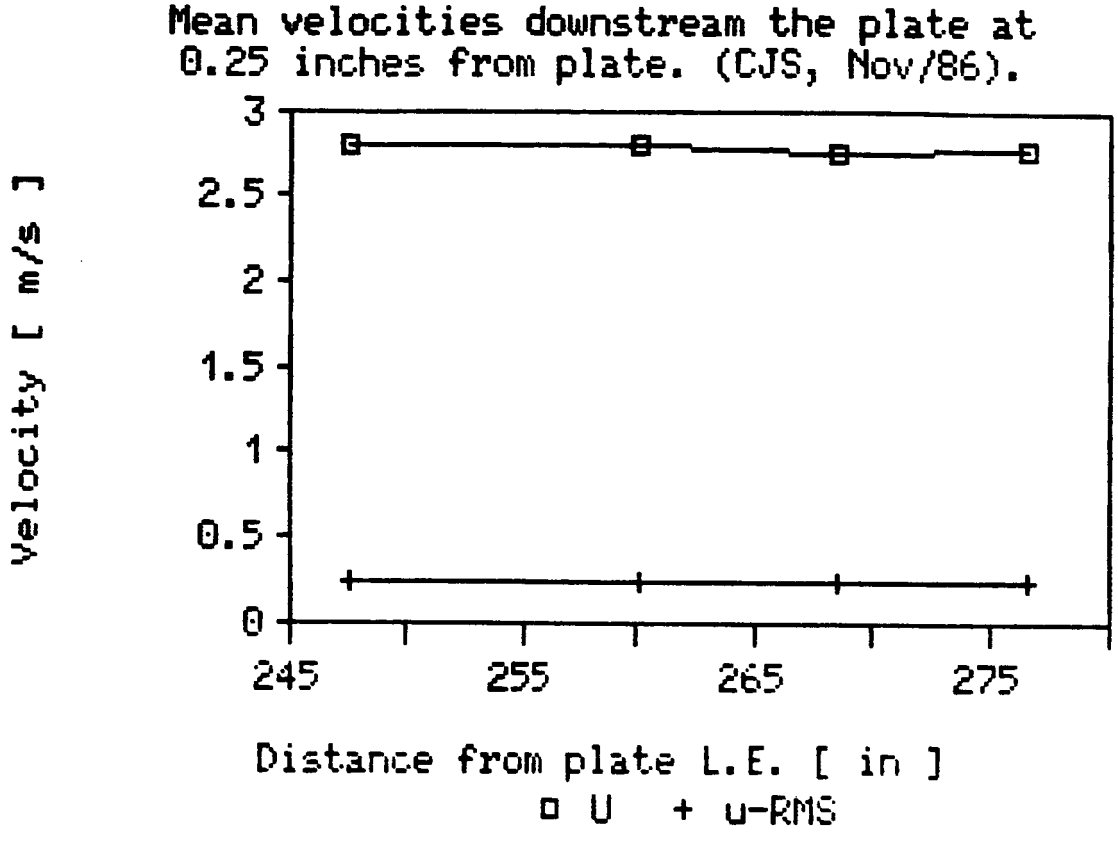

Figure 16. Splitter plate undulation determination using a single hot-wire (longitudinal).

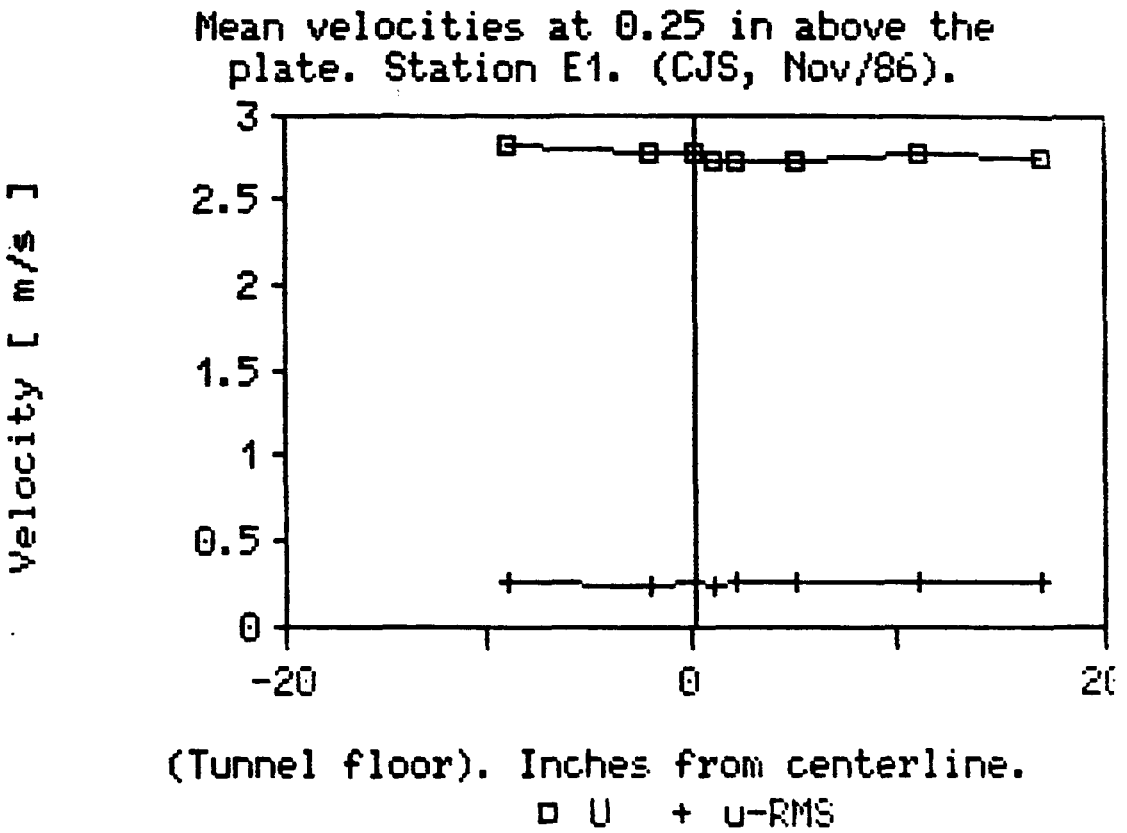

Figure 17. Splitter plate undulation determination using a single hot-wire (tranverce).

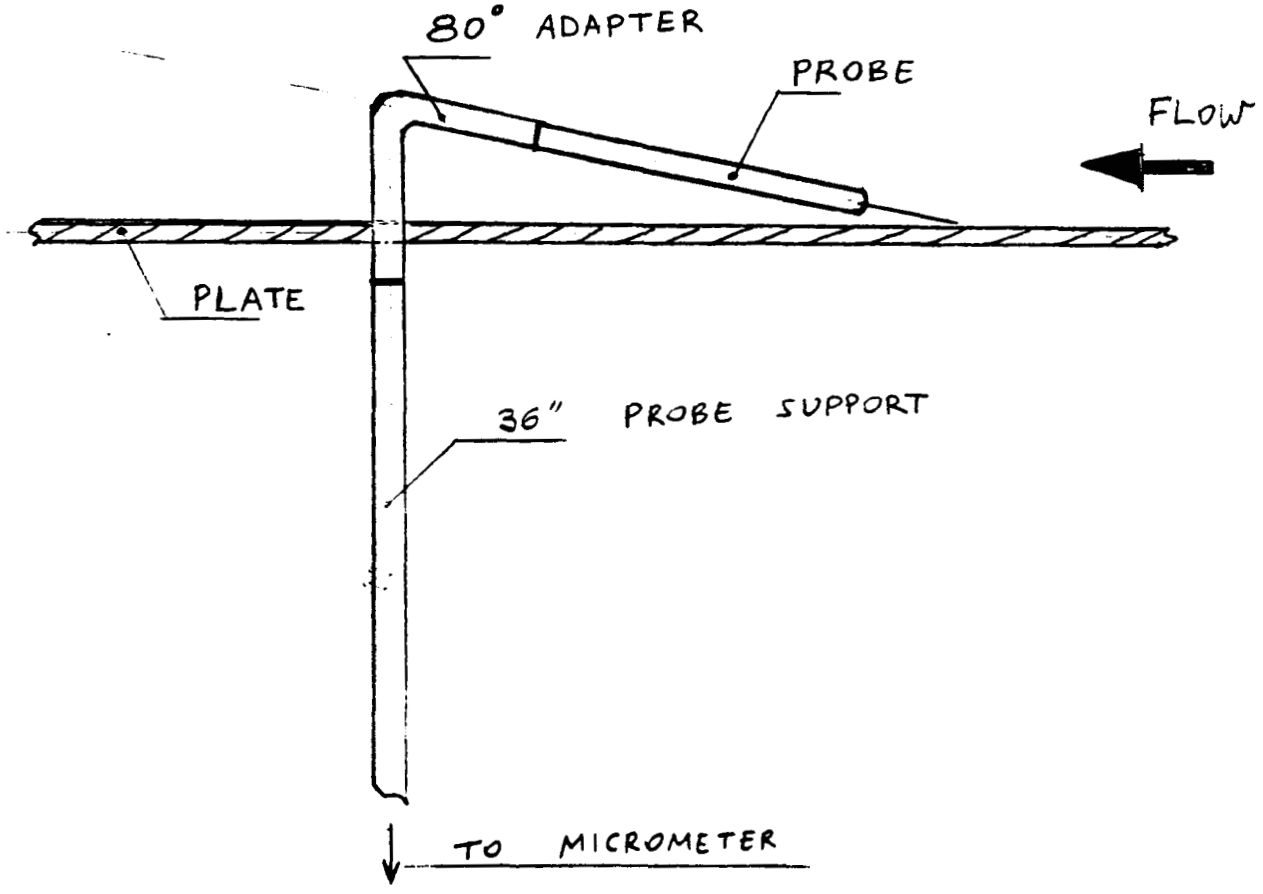

Figure 18. Single hot-wire placed over the splitter plate for near-wall measured.

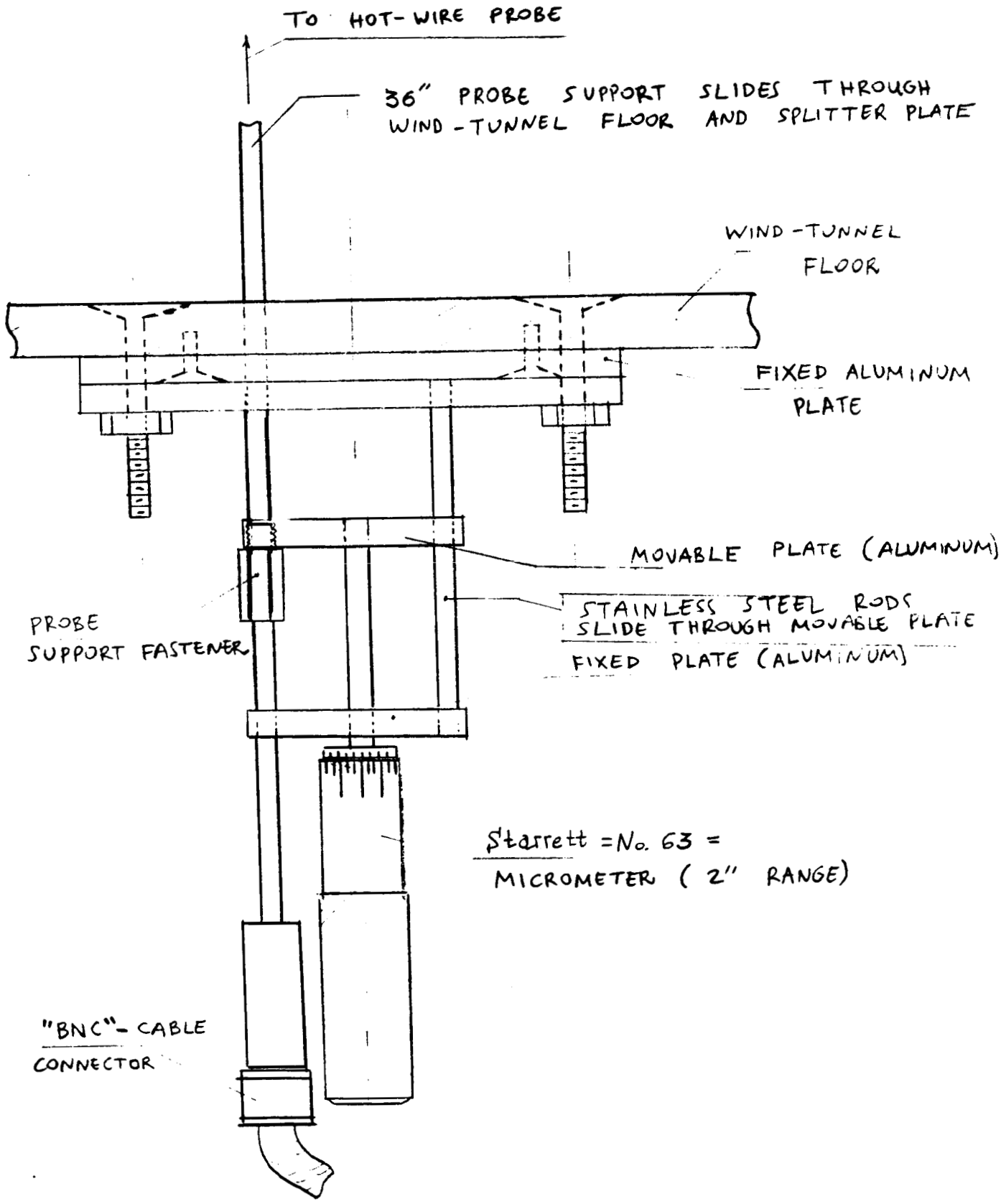

Figure 19. Near-wall positioning mechanism.

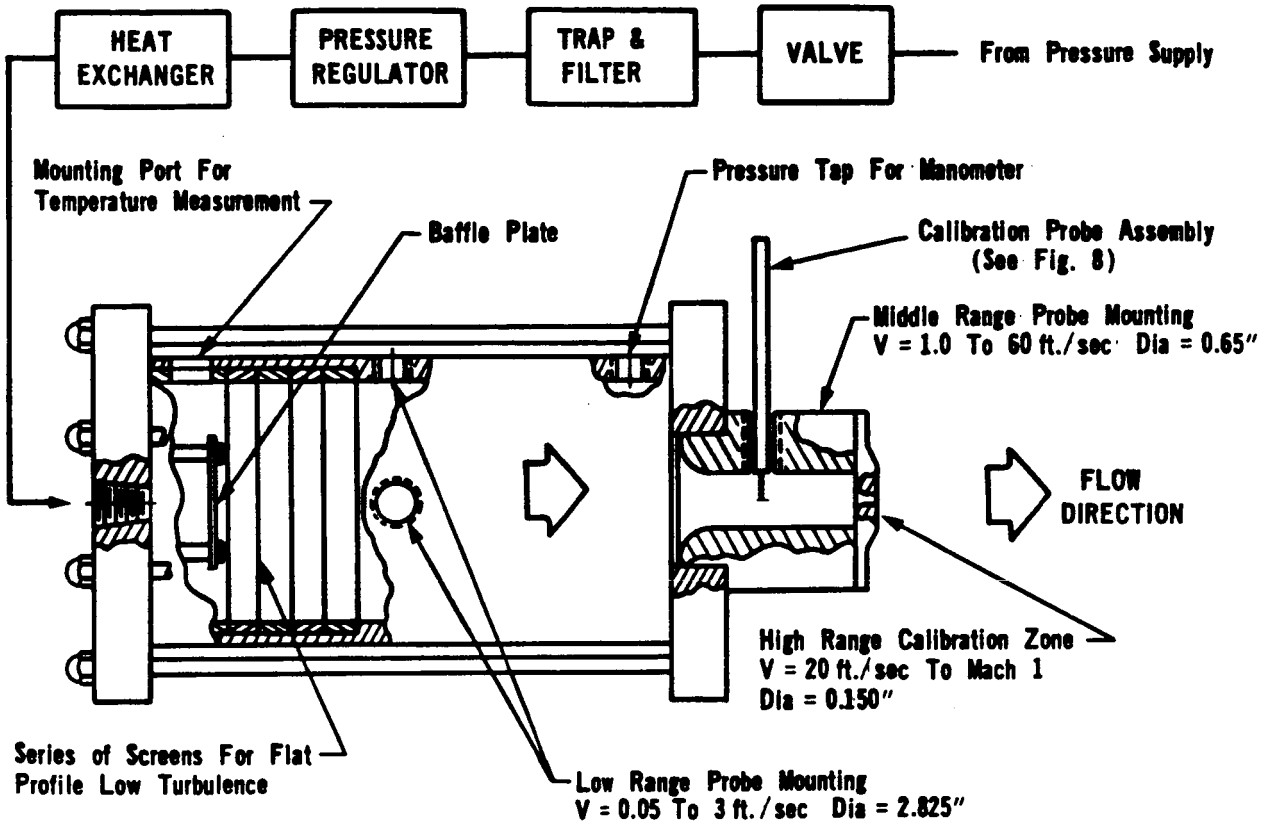

Figure 20. TSI calibrator (model # 1125) with a straight single hot-wire probe mounted.

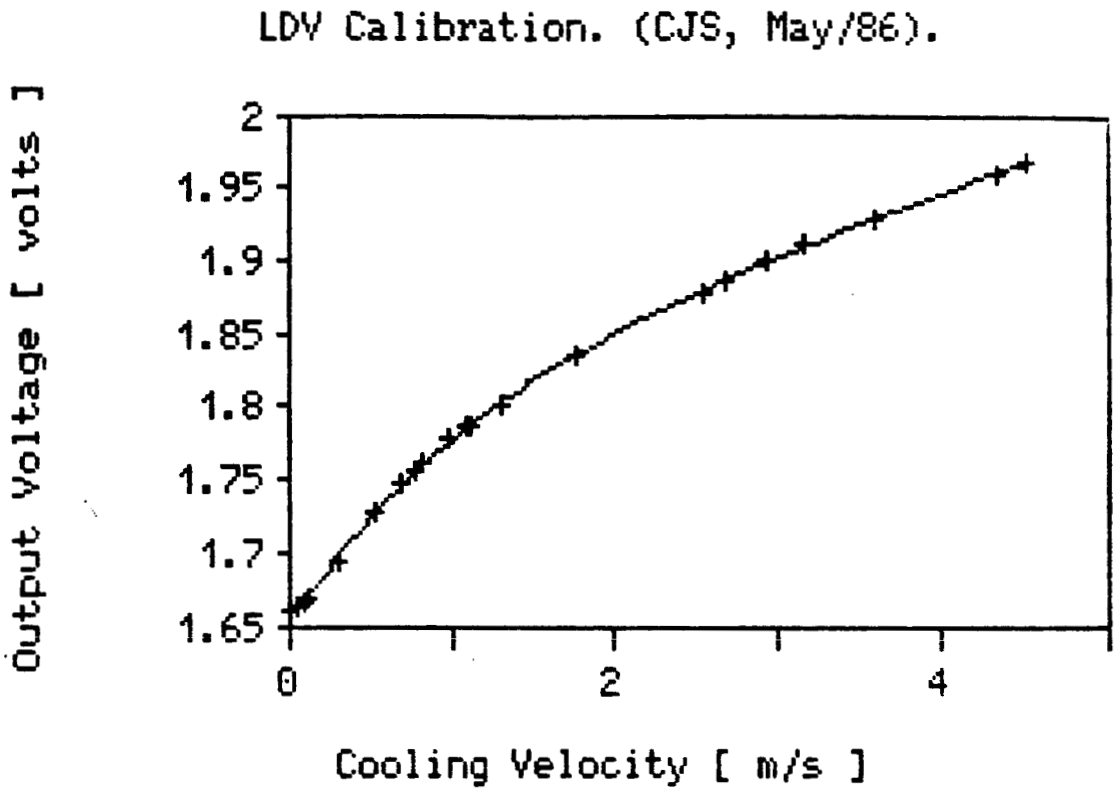

Figure 21. Single hot-wire calibration using LDV.

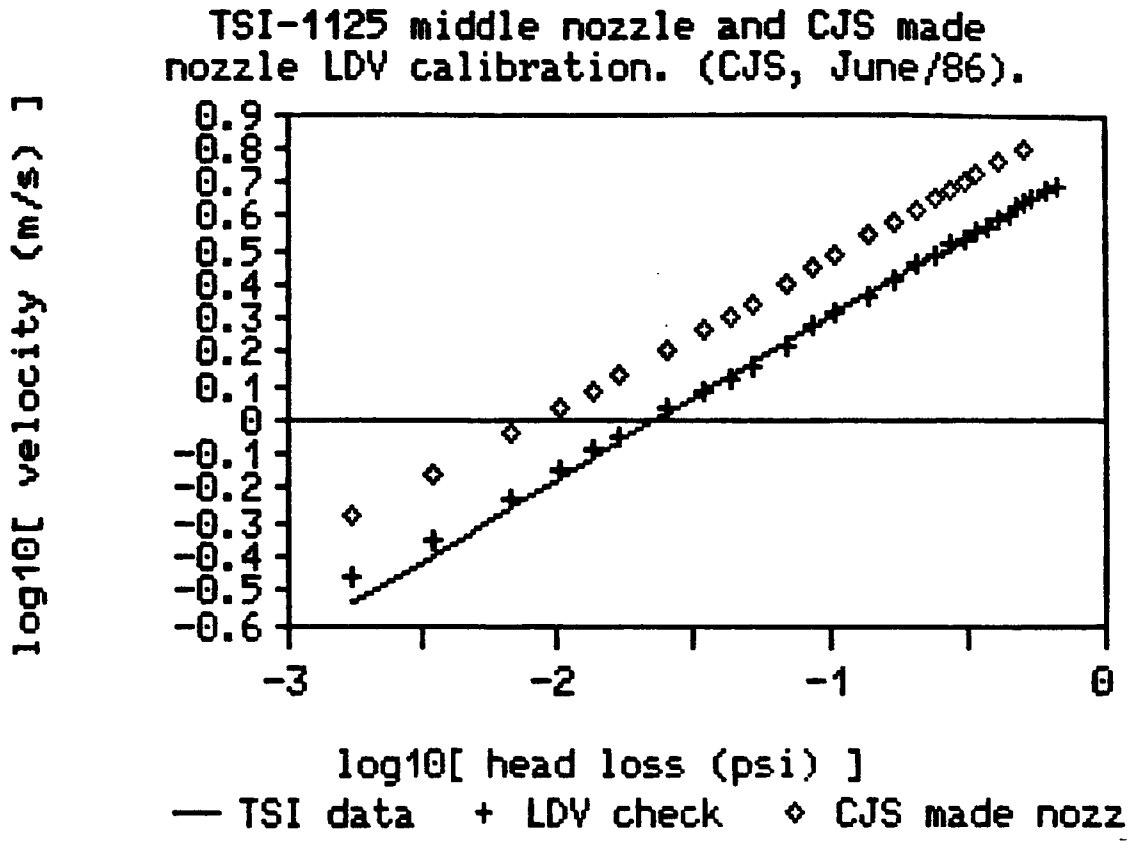

Figure 22. LDV calibration curves for the TSI calibrator. Line is the TSI supplied data.

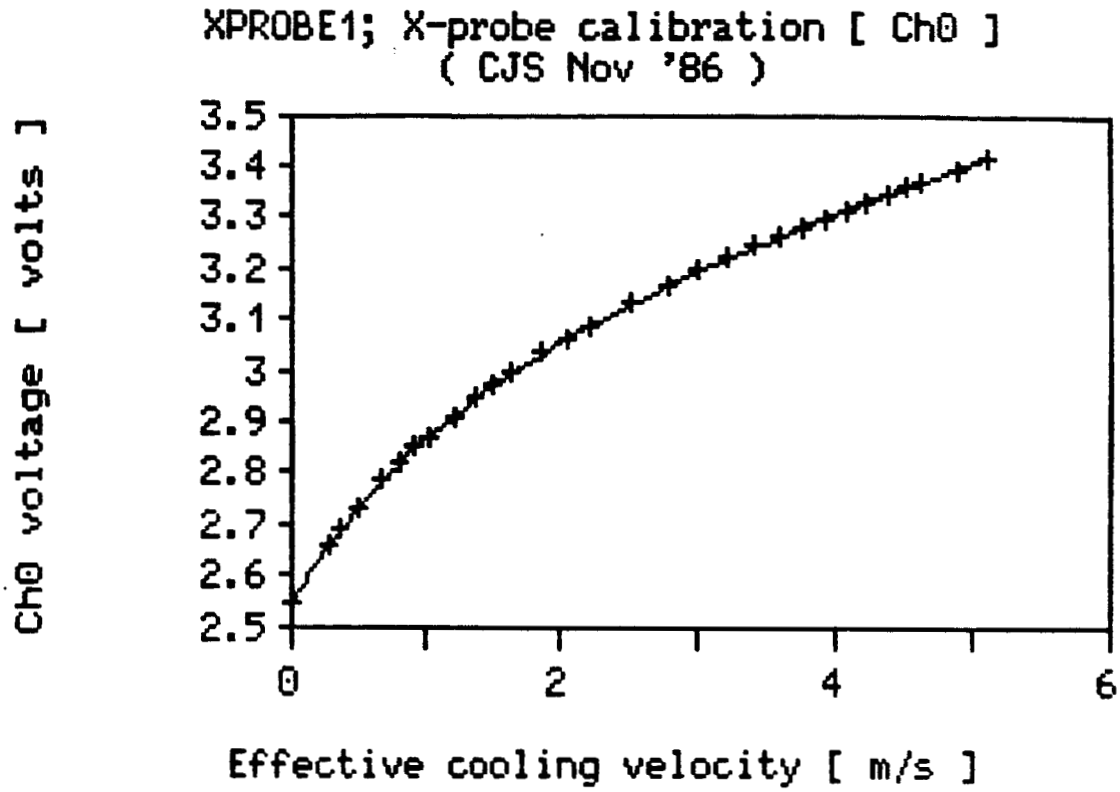

Figure 23. X-probe channel 0 calibration curve.

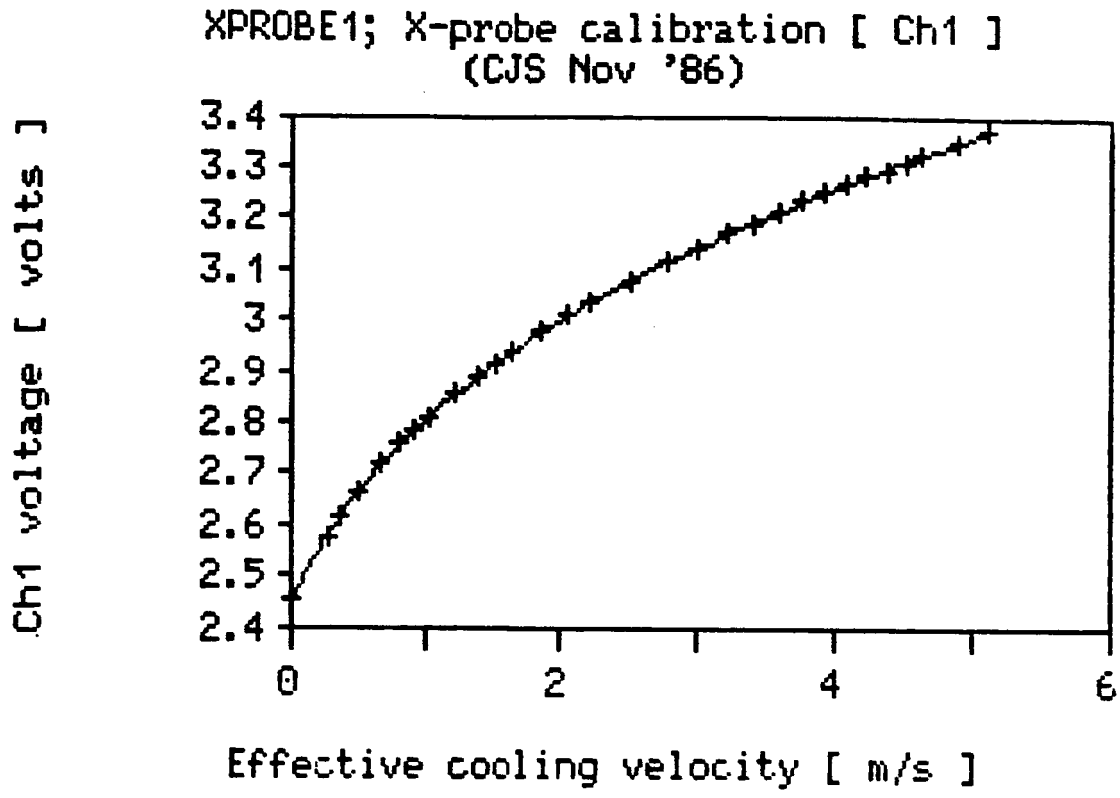

Figure 24. X-probe channel 1 calibration curve.

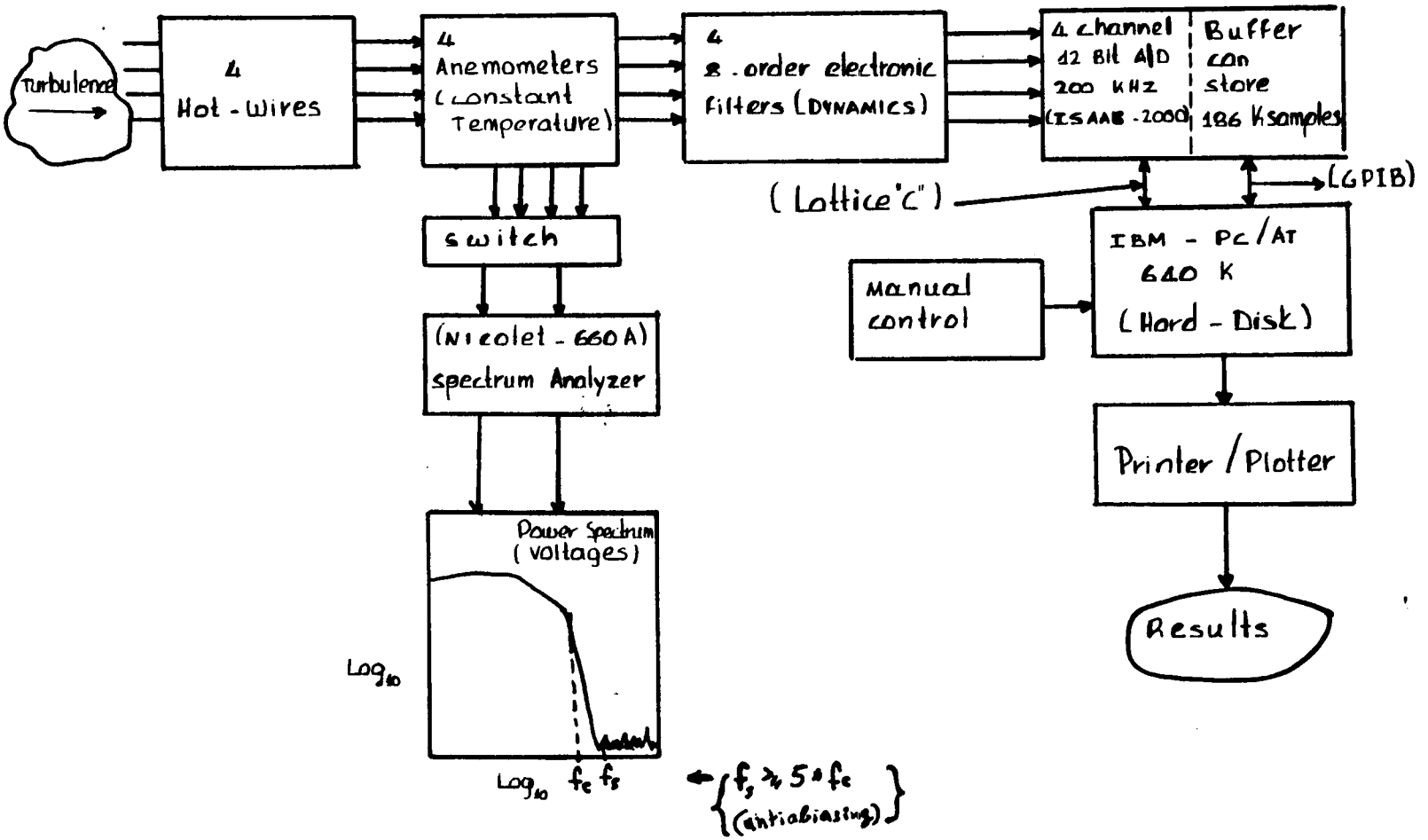

Figure 25. UCD wind-tunnel facility instrumentation.

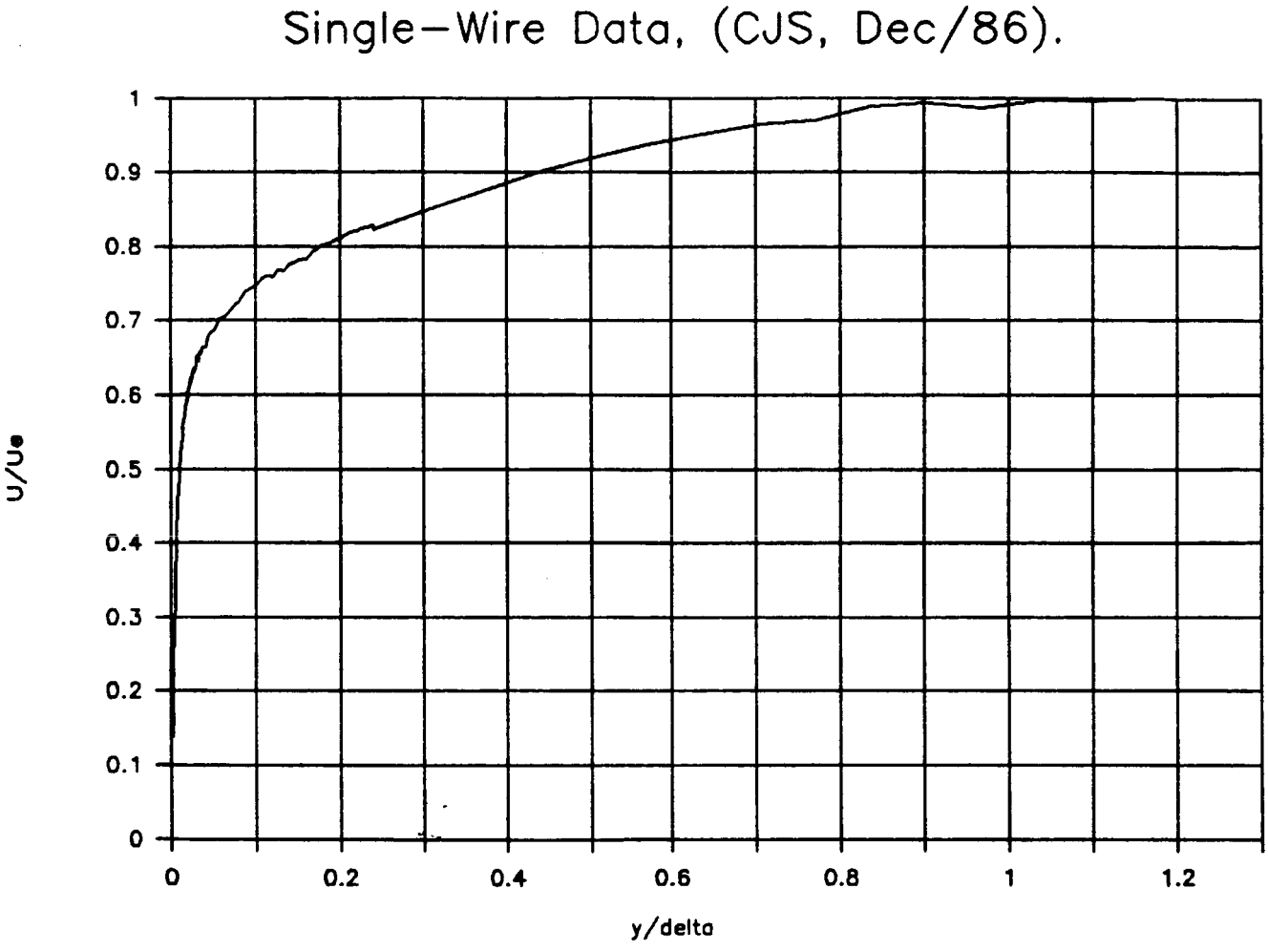

Figure 26. Dimensionless mean velocity distribution.

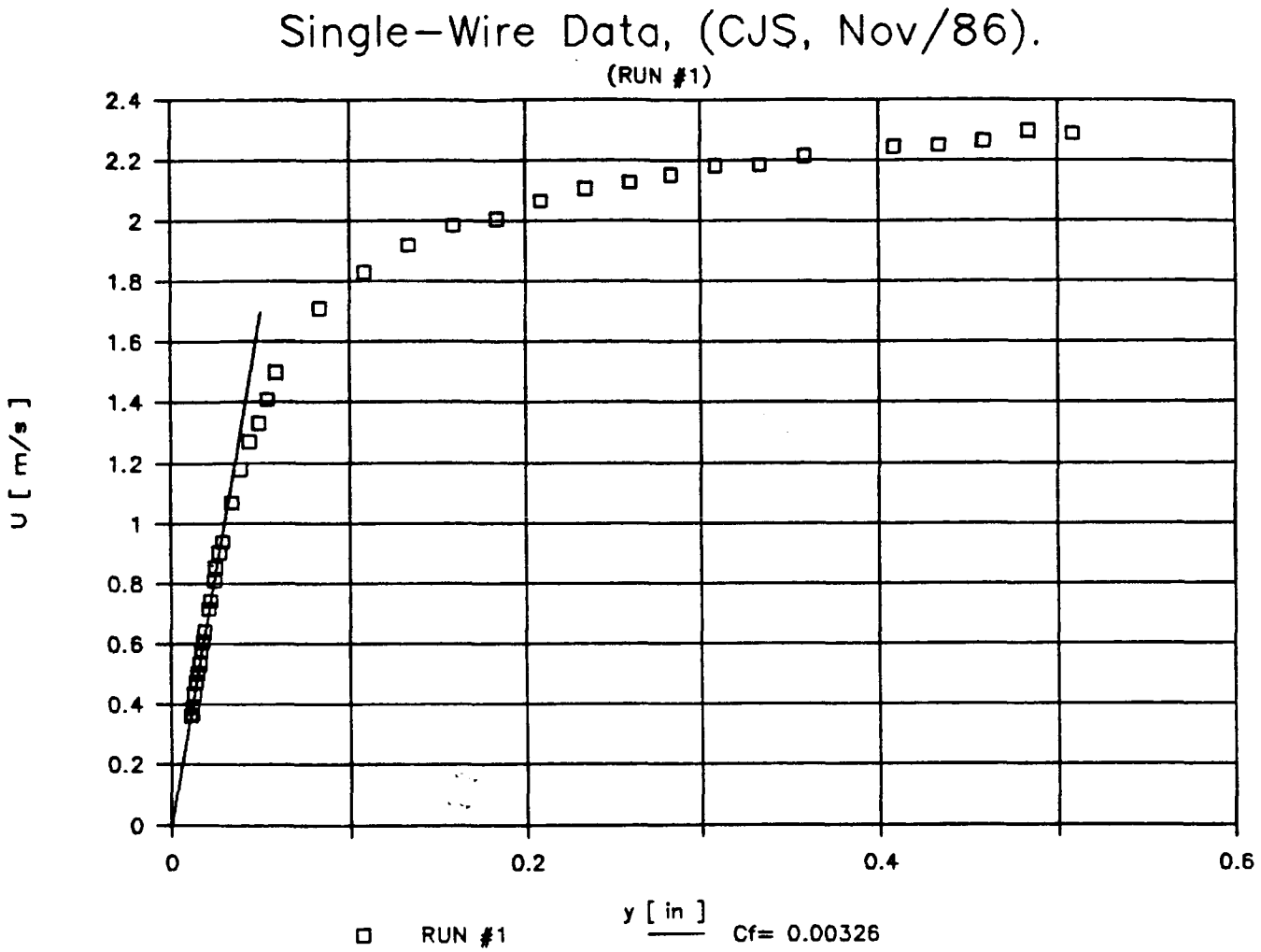

Figure 27. Near-wall detail of a mean velocity profile. Line represents the tangent to the profile at the wall.

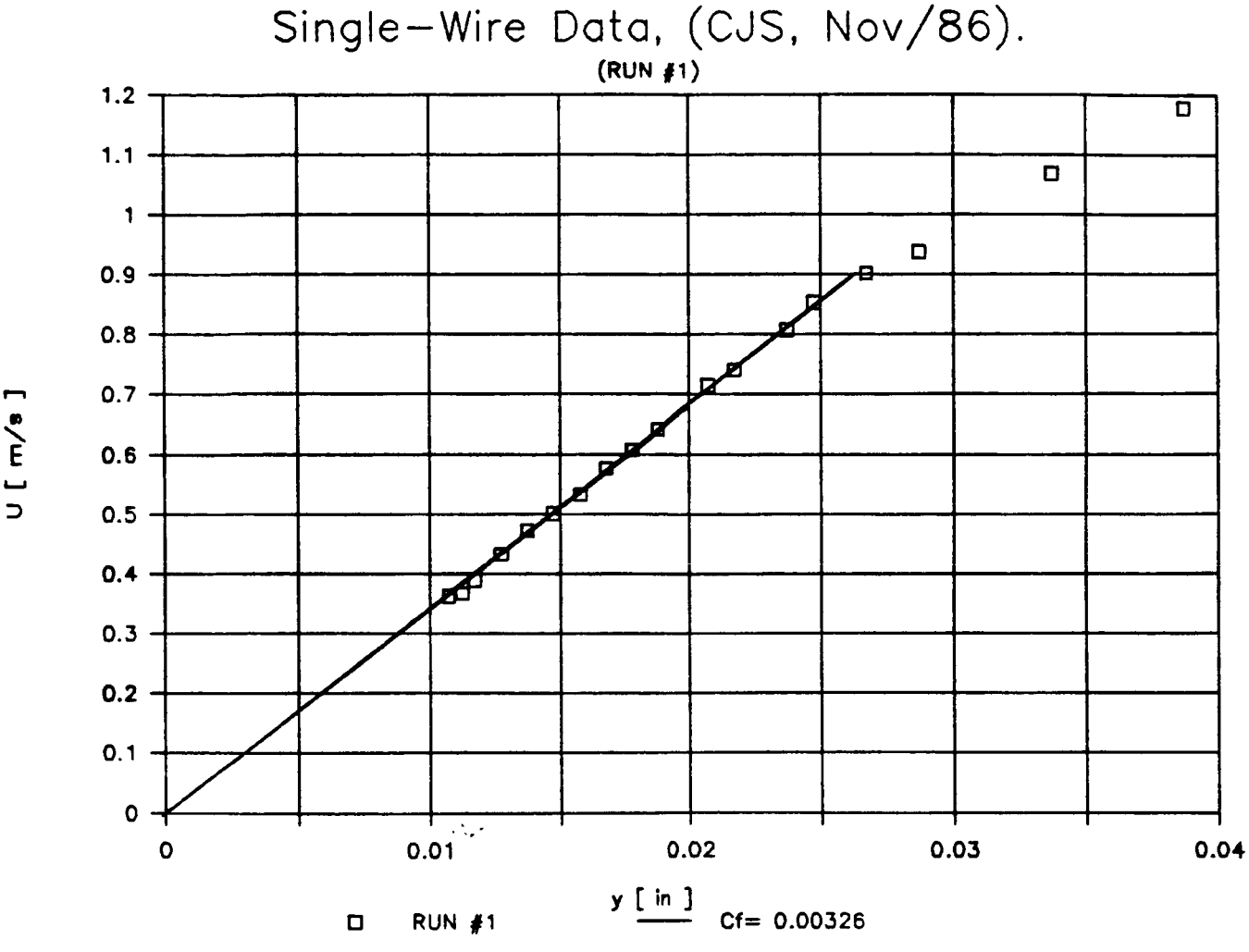

Figure 28. Mean velocity distribution. Viscous sublayer detail. Line for skin-friction coefficient estimation.

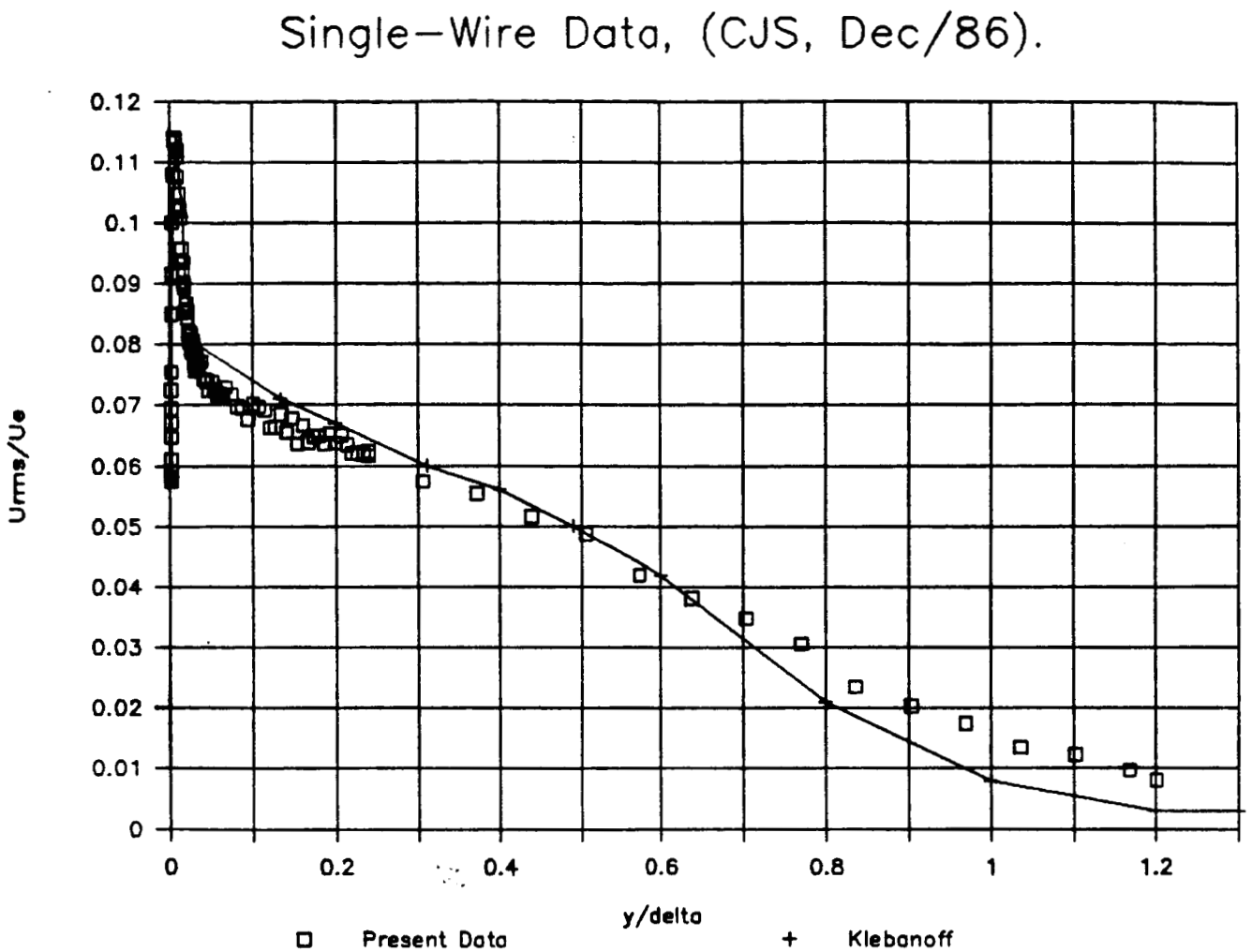

Figure 29. Turbulence distribution measured with a single hot-wire. Line is data by Klebanoff 1955.

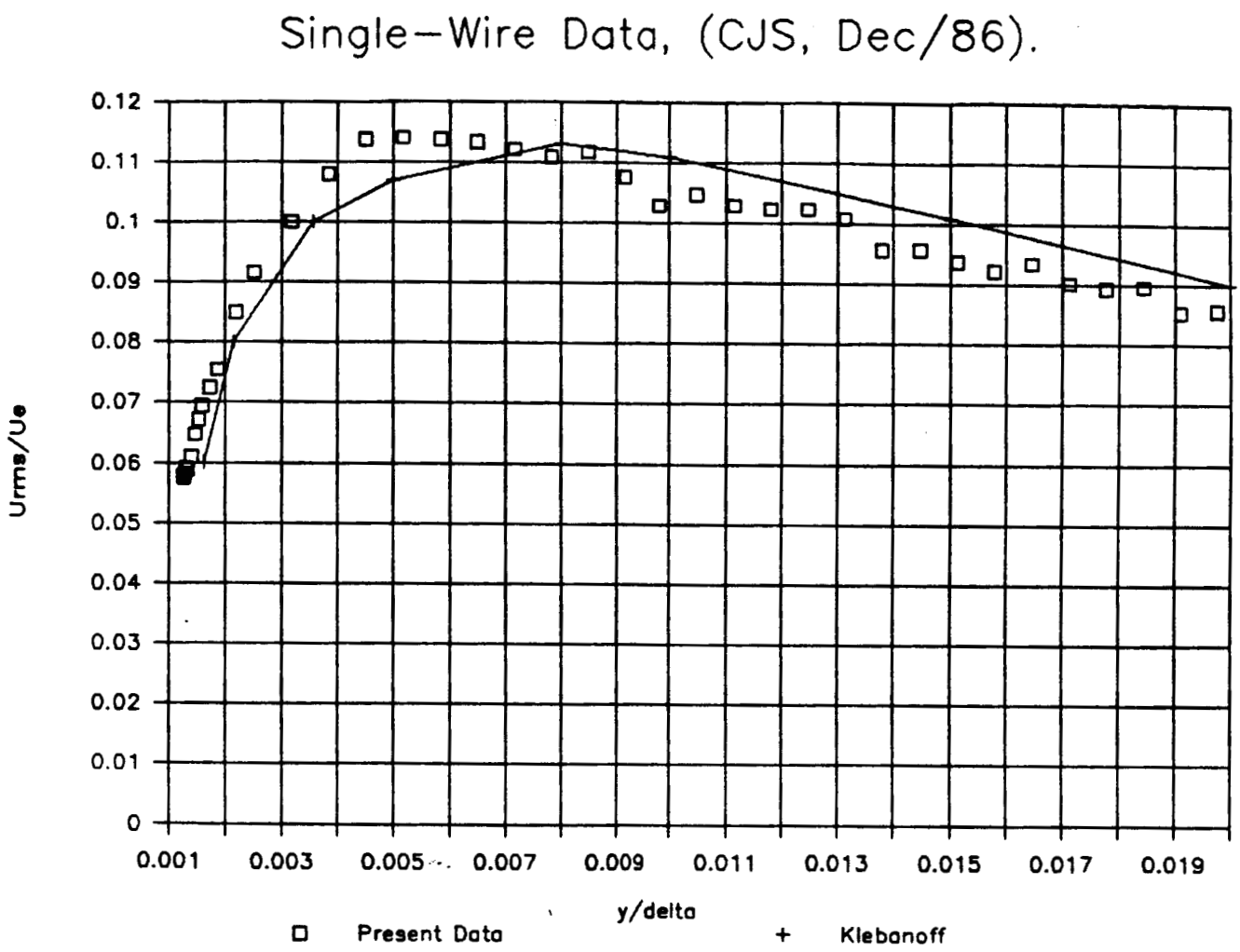

Figure 30. Near-wall detail of turbulence distribution measured with a single hot-wire. Line is data by Klebanoff 1955.

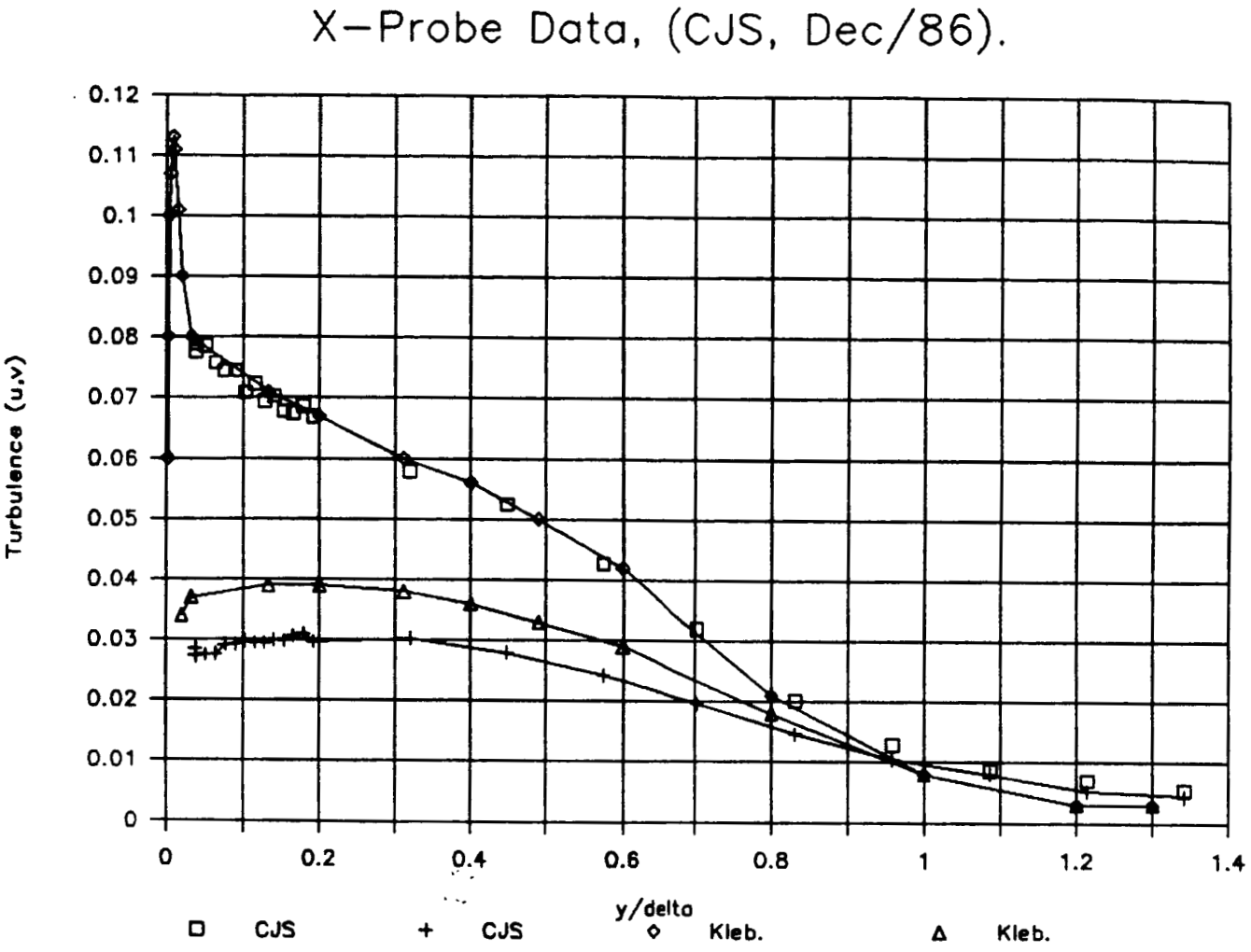

Figure 31. u and v turbulence distribution measured with crossed hot-wires. Comparison with Klebanoff's 1955 data.

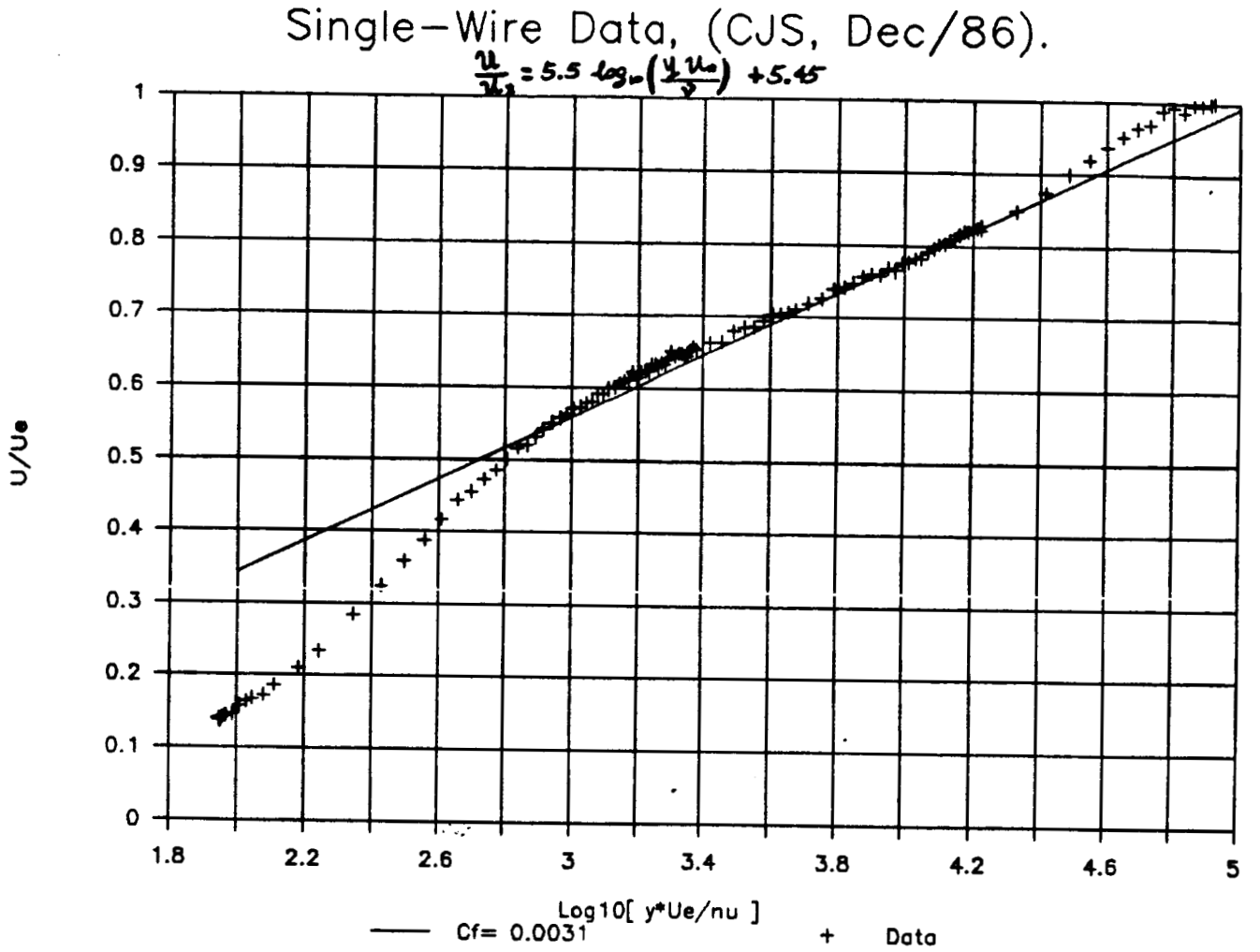

Figure 32. Clauser method for determining skin friction coefficient.

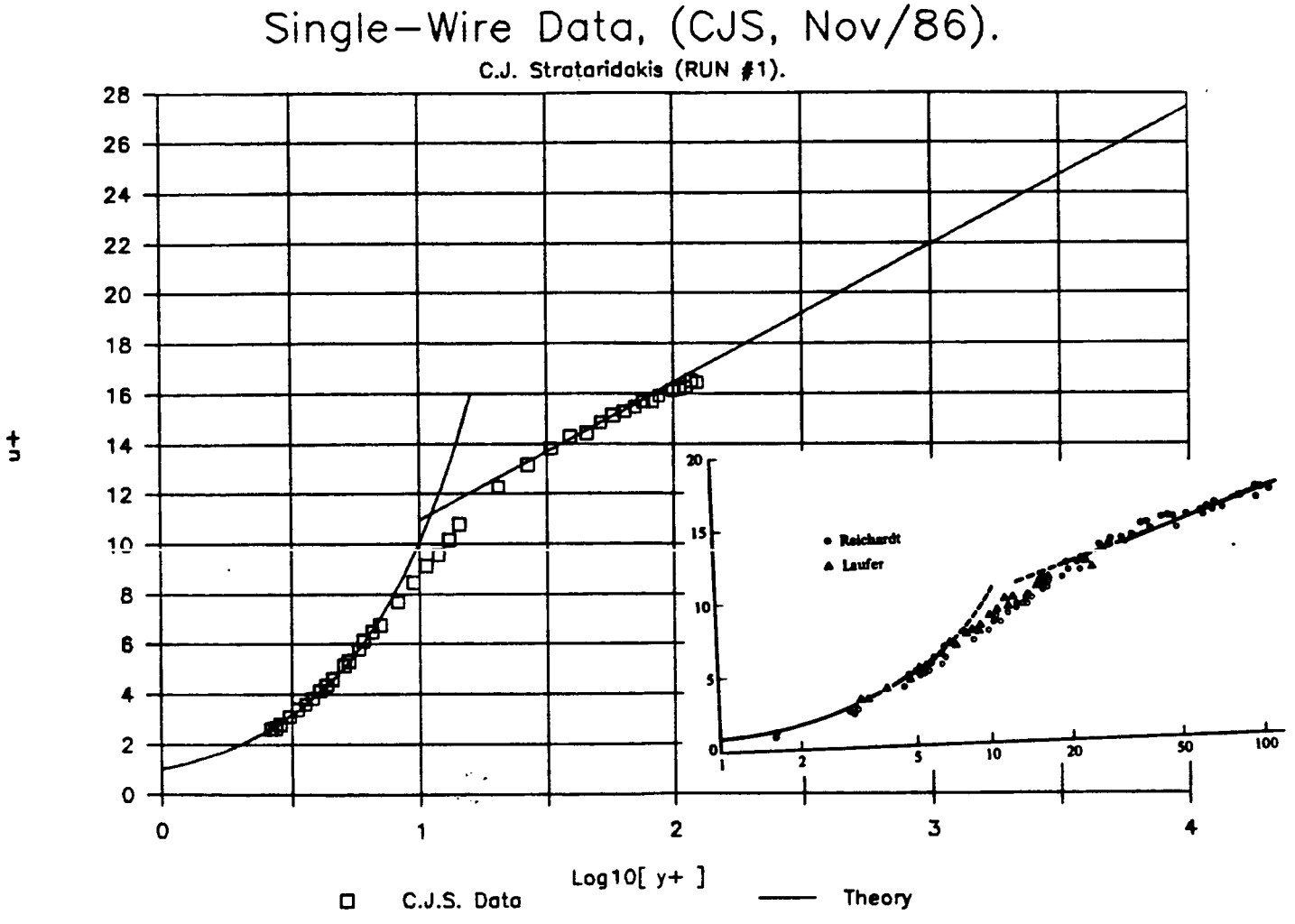

Figure 33. Near-wall mean velocity profile normalized by the friction speed.

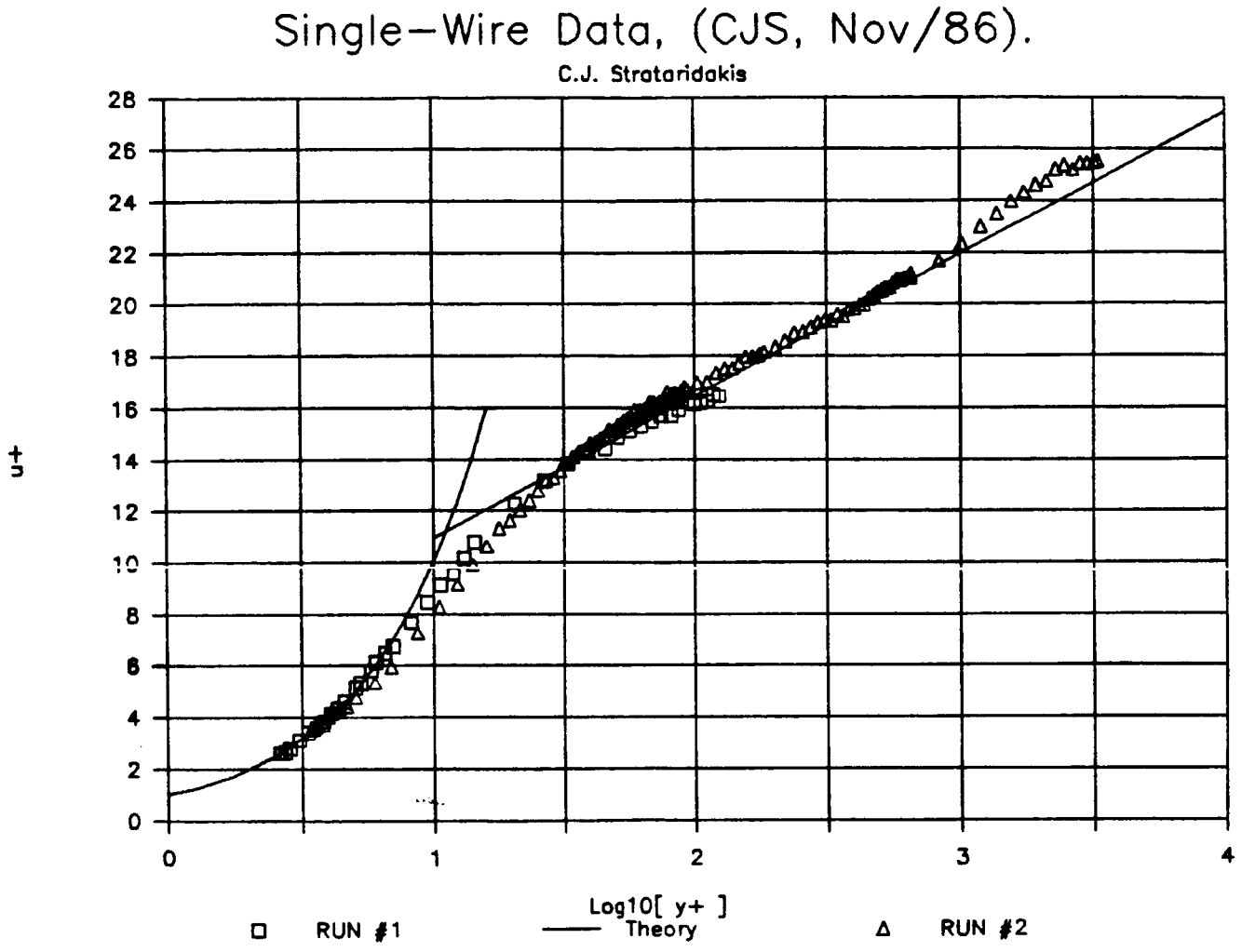

Figure 34. Near-wall mean velocity profiles normalized by the friction speed.

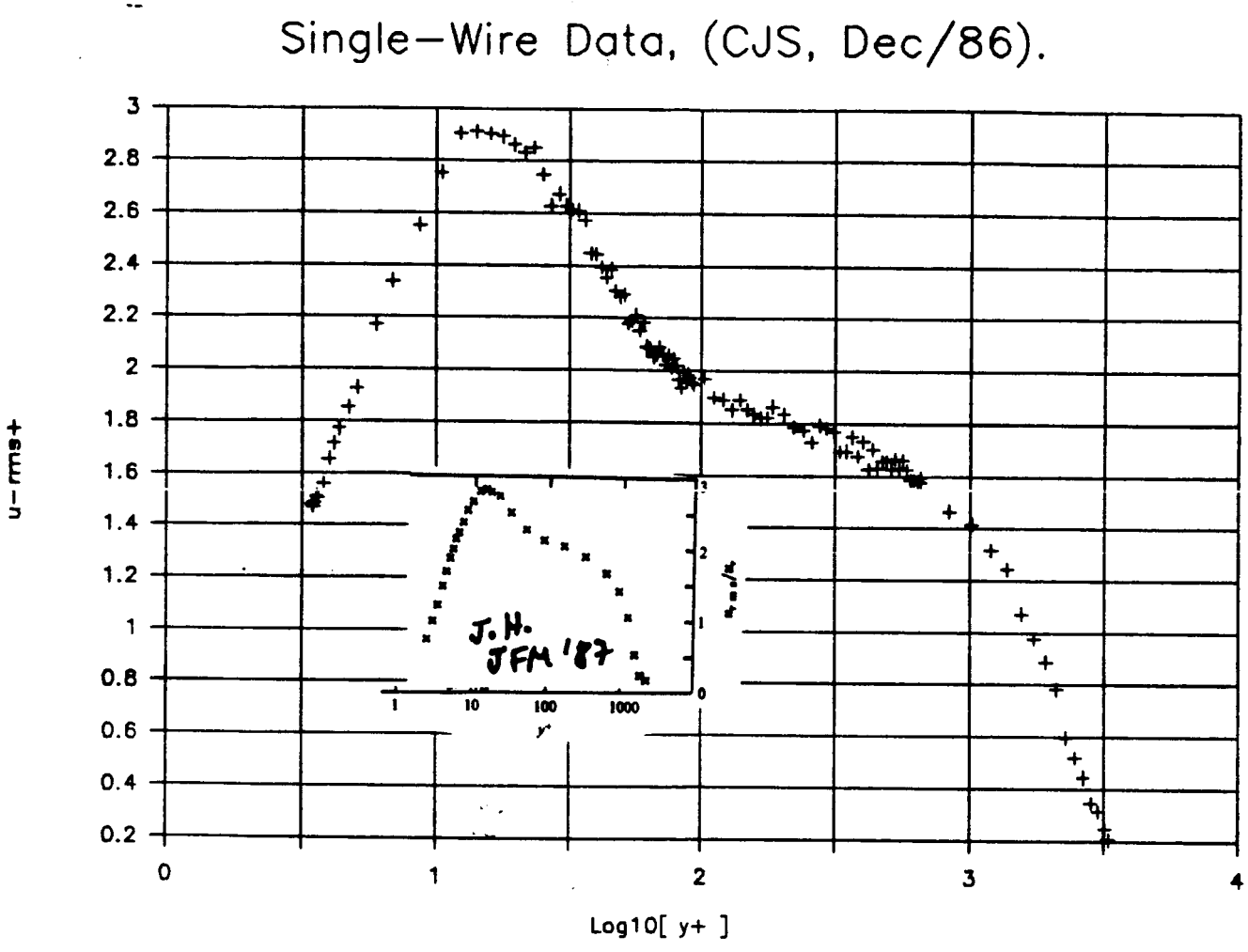

Figure 35. Turbulence data normalized by the friction speed. In window Haritonidis data.

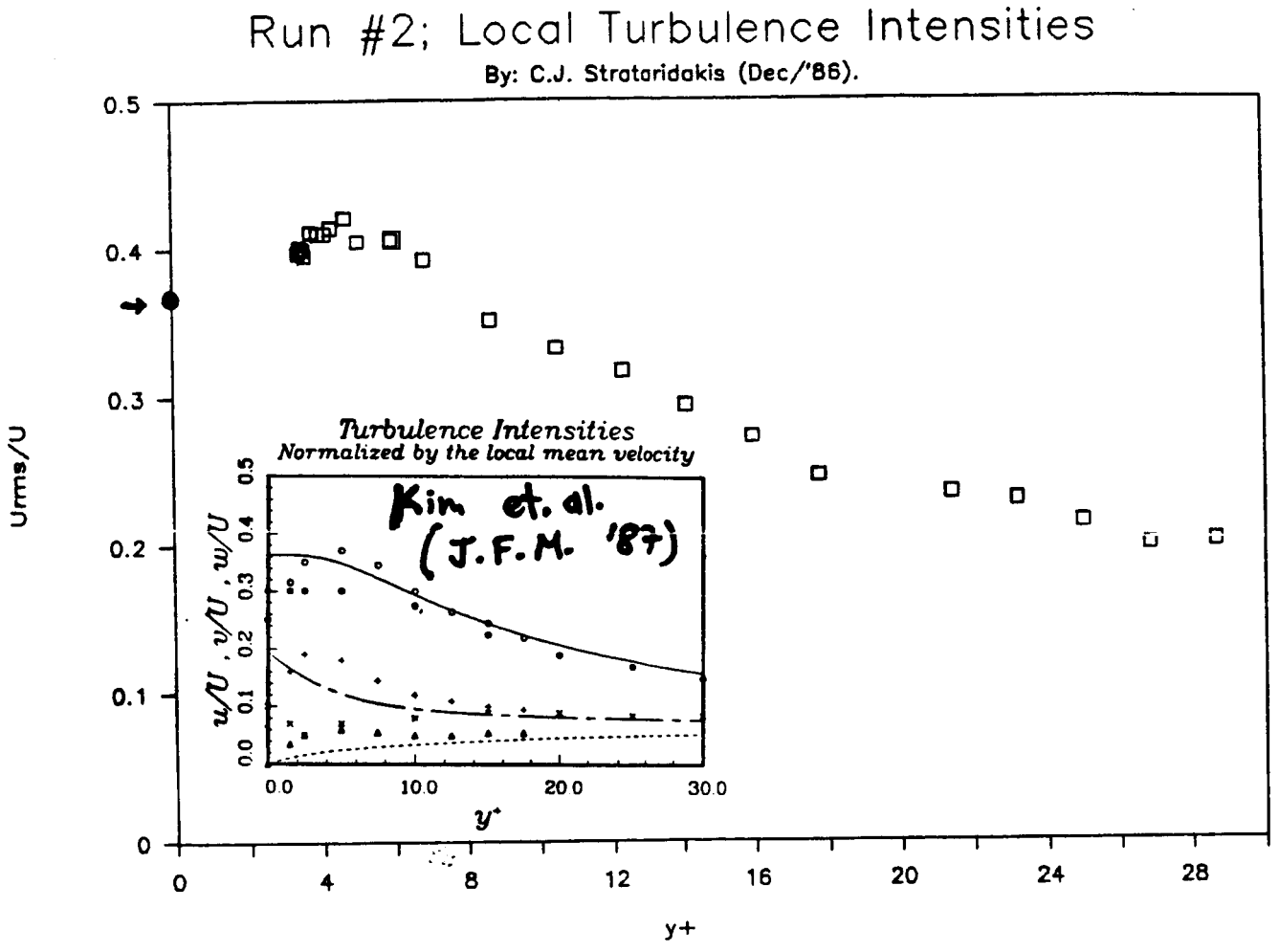

Figure 36. Longitudinal turbulence intensity near the wall normalized by the local mean velocity. In window data by Kim et. al. 1987.

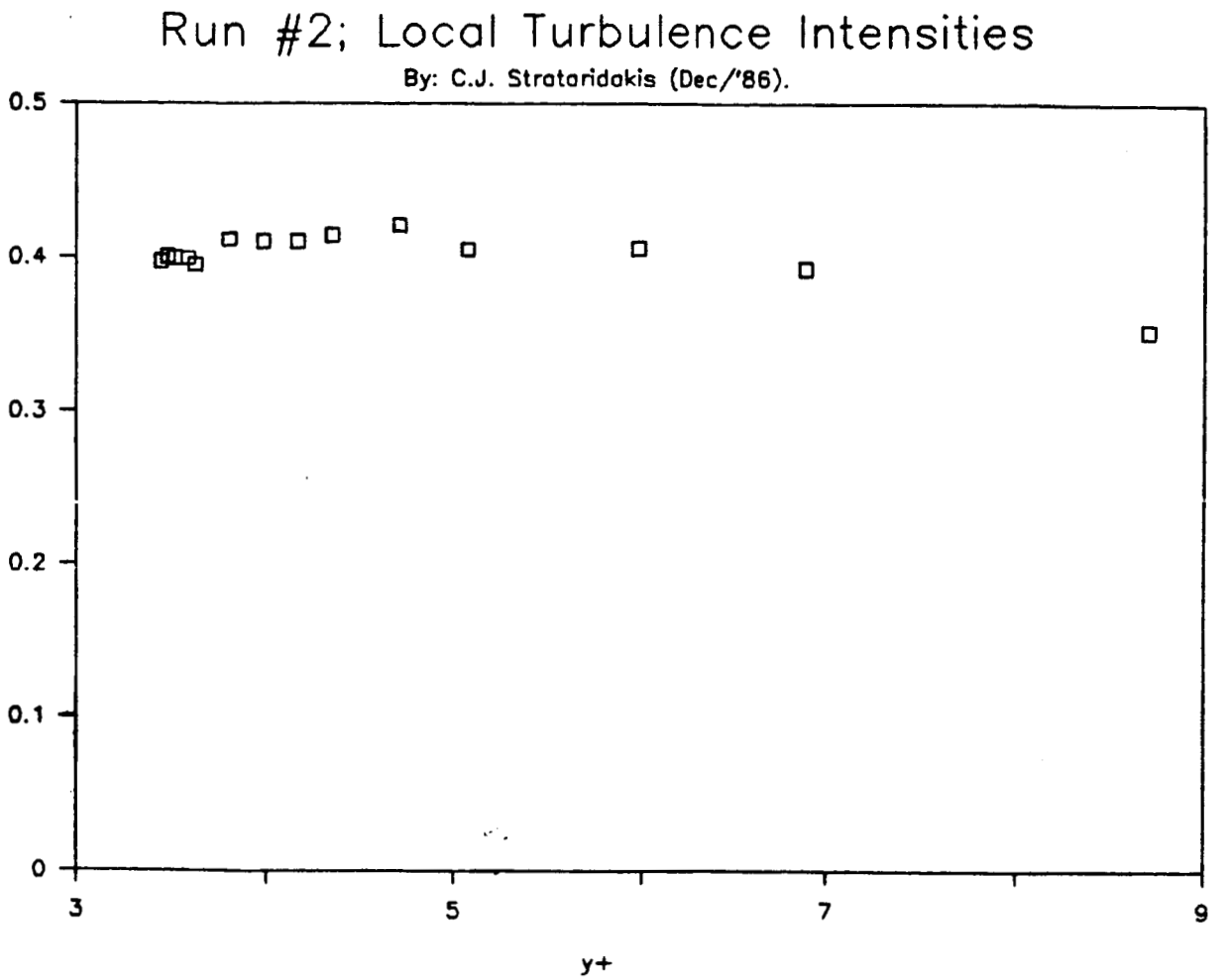

Figure 37. Longitudinal turbulence intensity near the wall normalized by the local mean velocity.

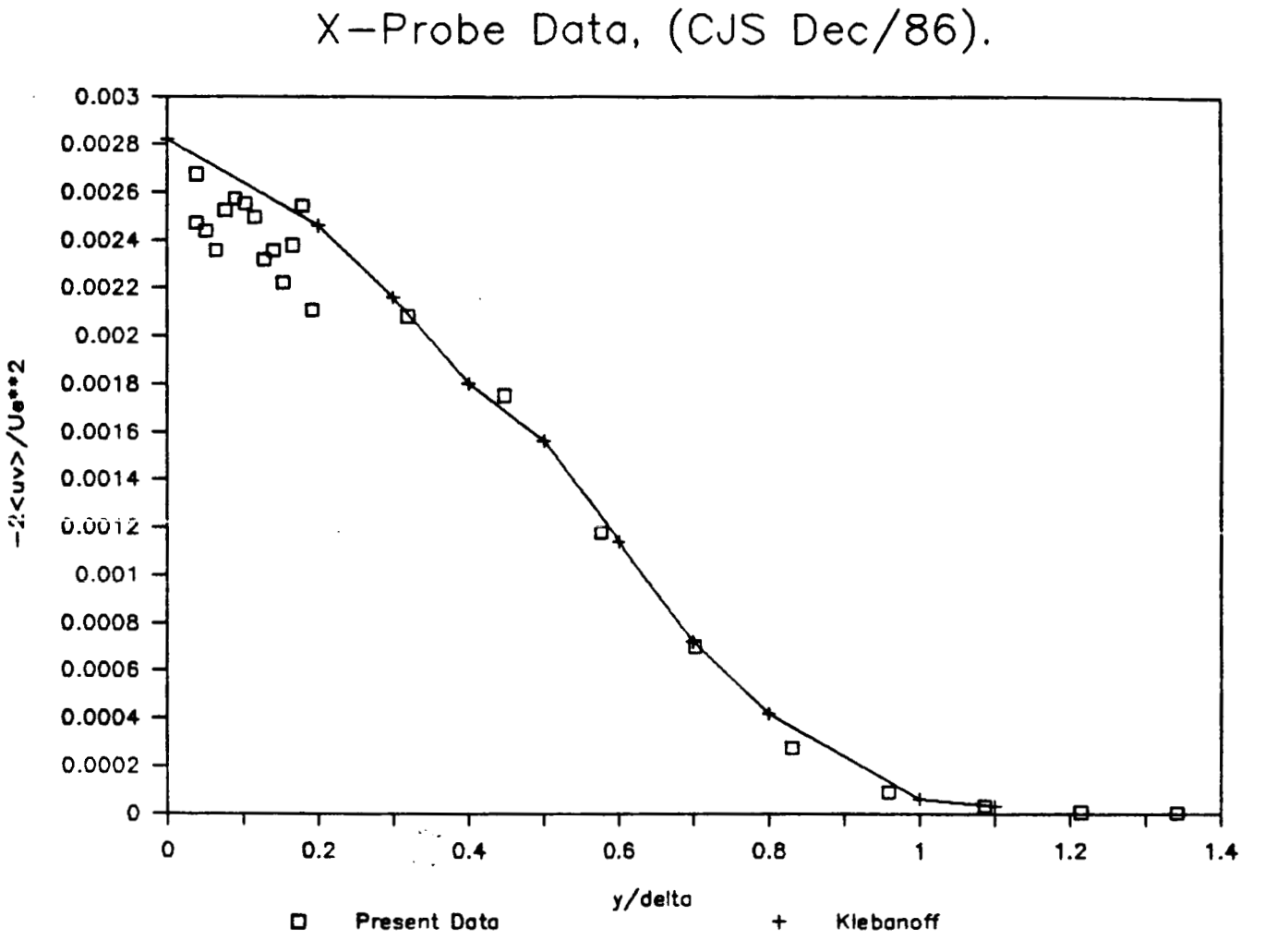

Figure 38. Shear-stress measured with a cross hot-wire probe. The line is data by Klebanoff 1955.

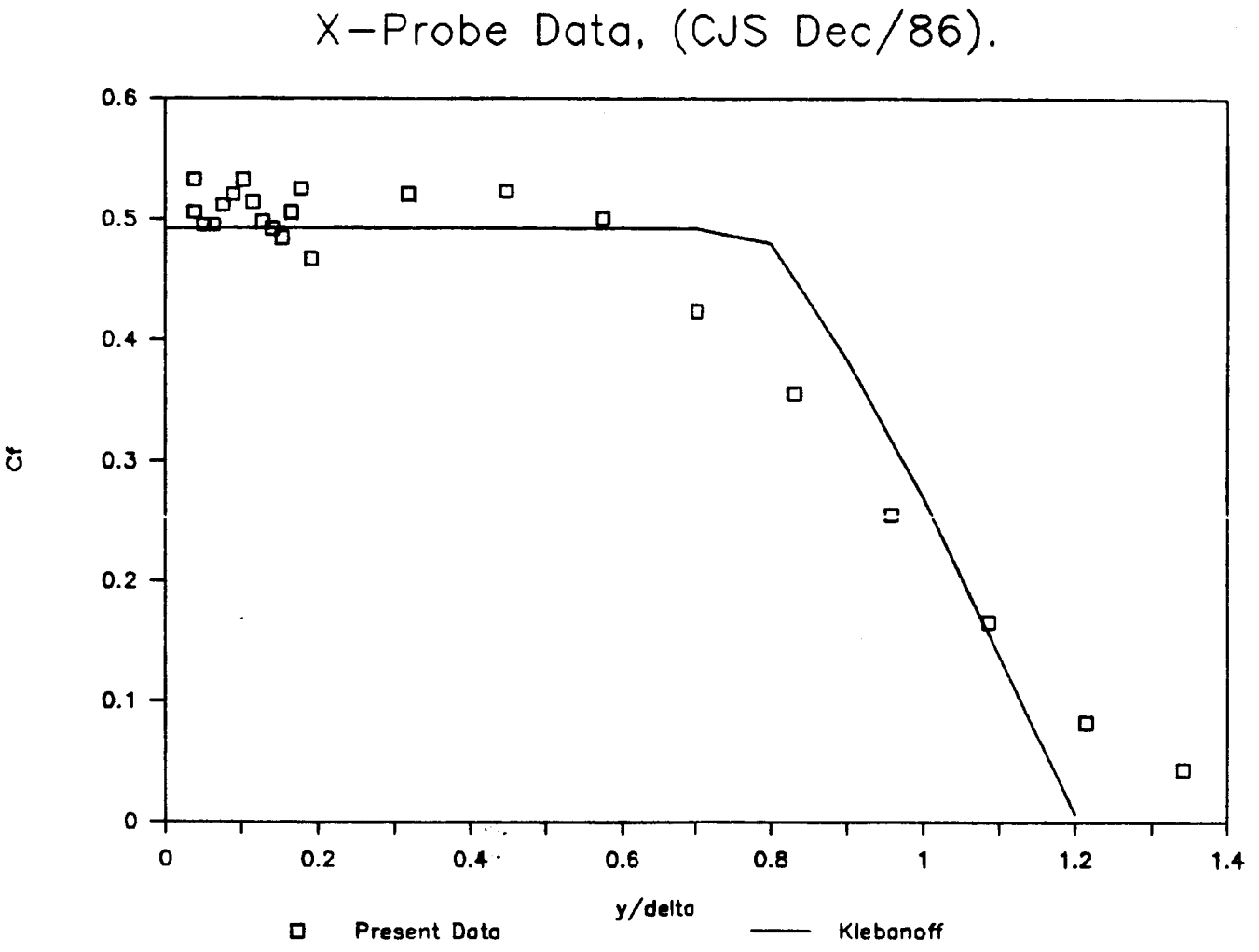

Figure 39. Cross-correlation coefficient as measured with a X-probe. The line is Klebanoff's result.

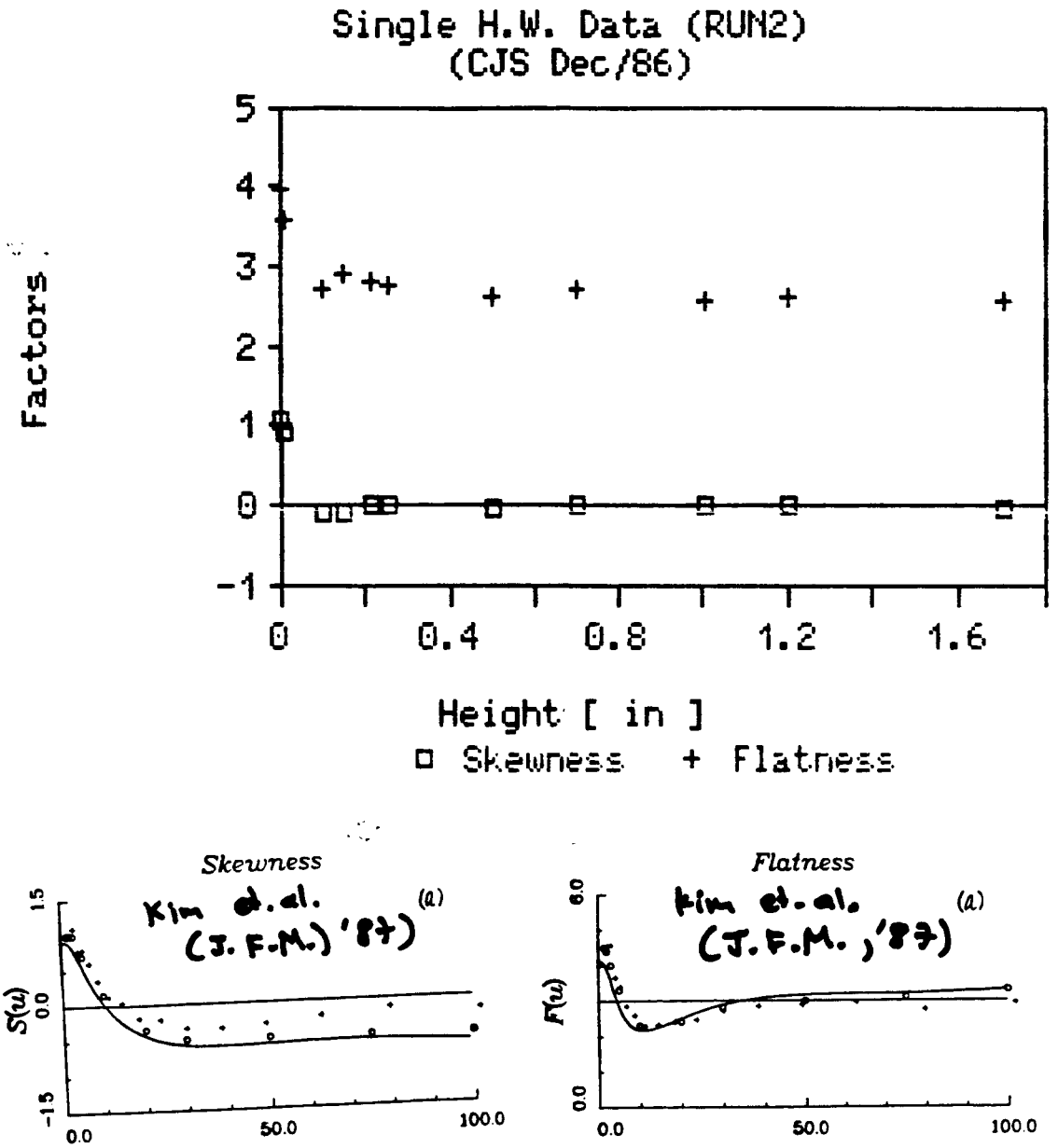

Figure 40. Near-wall skewness and Flatness as compares with Kim et. al. 1987 calculations.

Turbulent Boundary Layer Characteristics

• Typical Values

U_∞ = 5.28 m/s

δ = 0.20 m

δ_1 = 0.0217 m

θ = 0.01659 m

H_{12} = $\frac{\delta_1}{\theta}$ = 1.3

Re_x ≈ 2.5×10^6

Re_θ = 6,041

Sublayer thickness ≈ 0.6 - 0.7 mm

C_f = 0.0032

u_τ = 0.21 m/s

$\frac{\nu}{u_\tau}$ = 70 μm

Freestream turbulence = 0.3 %

$\frac{dP}{dx}$ = 0

Table 1. Turbulent boundary layer characteristics.